Thin film composite membranes based on a polymer of intrinsic microporosity derived from Tröger's base: A combined experimental and computational investigation of the role of residual casting solvent

Thin film composite membranes based on a polymer of intrinsic microporosity derived from Tröger's base: A combined experimental and computational investigation of the role of residual casting solvent

Paola Bernardo[a], Valentina Scorzafave[a], Gabriele Clarizia[a*], Elena Tocci[a*], J.C. Jansen[a], Andrea Borgogno[b], Richard Malpass-Evans[c], Neil B. McKeown[c], Mariolino Carta[d], Franco Tasselli[a]

a) Institute on Membrane Technology, ITM-CNR, c/o University of Calabria, Via P. Bucci 17/C, 87036 Rende (CS), Italy
b) Institute of Biomolecular Chemistry, ICB-CNR, Via F. Marzolo 1, 35131 Padova, Italy
c) EaStCHEM, University of Edinburgh, School of Chemistry, Joseph Black Building, David Brewster Road, Edinburgh, EH9 3FJ, UK
d) Swansea University, Department of Chemistry, College of Science, Grove Building, Singleton Park, Swansea, SA2 8PP, UK

**Corresponding authors*: g.clarizia@itm.cnr.it; e.tocci@itm.cnr.it

Keywords: Thin film composite membranes; molecular dynamics; gas separation; PIM-EA(H_2)-TB

Abstract

Composite membranes were developed for gas separation applications, both as flat-sheets and hollow fibres, using a Polymer of Intrinsic Microporosity, composed of Tröger's base, TB, and of ethanoanthracene (PIM-EA(H_2)-TB) as the selective layer. The crucial role of the solvent, dichloromethane and chloroform, used in membrane preparation on the transport properties was evaluated by both thermogravimetric analysis and permeation tests on PIM-EA(H_2)-TB dense self-supported films. Molecular modelling, reproducing the experimental conditions in presence of the two different solvents, was performed to investigate the role of the solvent on the morphological and transport properties of the PIM polymer. The strong interaction of the polymer matrix with chloroform reduces gas permeability due to the partial saturation of the sorption sites and the competition between solvent and permeating gas molecules. Consequently, dichloromethane was chosen as suitable solvent in composite membrane preparation also for its good compatibility with PAN. PAN-based hollow fibres were prepared according to phase inversion method and used as porous supports. They were functionalised by partial conversion of the nitrile groups into carboxyl groups to improve compatibility with the active PIM layer. Controlled temperature and humidity conditions during the coating process reduced the presence of micropores on the membrane surface, favouring the formation of a dense layer on the hollow fibre porous support. Composite PIM-EA(H_2)-

TB membranes were successfully developed having selectivity similar to the dense membranes for different gas pairs.

Introduction

Polymeric membranes play an increasingly important role in gas separations [1]. The design of polymers with an increased chain rigidity, as suggested by Freeman [2], such as the Polymers of Intrinsic Microporosity (PIMs) [3], has provided better performing materials relative to the Robeson upper bounds, which define the state of the art in the trade-off between permeability and selectivity [4]. PIMs are relatively inflexible and contorted macromolecules. Their fused ring sequences, interrupted by contortion sites, ensure high free volume through increasing inter-chain separation. The result is a high gas diffusivity, coupled with enhanced solubility and hence high permeability [3, 5]. Recently, the synthesis and gas permeability of PIM-EA-TB, composed solely of benzene rings and bridged bicyclic units based on Tröger's Base (TB) and ethanoanthracene (EA), was reported [6, 7]. PIM-EA-TB demonstrates a distinct size-sieving behaviour, with the preferential permeation of H_2 with respect to CO_2, surpassing the Robeson's upper bound in the case of O_2/N_2, H_2/N_2 and H_2/CH_4 gas pairs [6, 7].

Membranes produced for practical application typically include a thin selective layer of the polymer performing the separation applied onto a porous and mechanically stable support [8, 9]. This composite configuration combines good selective properties and high fluxes, thus reducing the use of expensive materials as the selective layer. However, the required thin layers could present defects that may affect selectivity [10]. Frequently, a "gutter layer" between the microporous support and the selective layer is included, to channel permeating molecules to the relatively widely spaced pores in the support [8, 9] and to allow a smooth defect-free surface to be coated. Hollow fibres are typically used in gas separation owing to their higher surface area-to-volume ratio, lower resistance to gas flow and the ability to support higher transmembrane pressure drops, when compared with flat membranes [10]. Coating conditions during the fabrication procedure greatly influence the gas separation performance of resulting membranes. Polymer concentration and solvent used in coating solution, along with substrate porosity, pre-wetting treatment and substrate materials all have to be carefully evaluated to produce thin defect-free coatings [11–13].

In this work, thin film composite membranes were developed using PIM-EA(H_2)-TB, a simple modification of the much studied polymer PIM-EA-TB, lacking two methyl groups on the EA unit [15]. The properties of PIMs-based membranes strongly depend on their preparation history (casting solvent, thermal treatment, ageing, etc.). In general, the casting solvent also has an important role in determining the free volume morphology of the membrane, exerting a key influence on the gas

transport (e.g., sorption, diffusion and permeation) [16]. The solvent properties may influence the final microstructure of a glassy polymer matrix via interaction with the polymer macromolecules, such as dipole-dipole interactions and hydrogen bonding [17-20]. PIMs, like other highly permeable polymers, tend to retain a considerable amount of casting solvent. Generally, soaking in methanol helps to reset the history of PIM samples since it swells the polymer, flushing out residual solvent and allowing relaxation of the polymer chains [21, 22]. However, the treatment with alcohols of composite membranes could induce a different swelling in the layers, resulting in the delamination of the coating. It should be avoided in thin film composite membranes, since a differential swelling in the layers could result in the membrane failure.

Therefore, an investigation of the role of the solvent used for casting the membranes based on PIM-EA(H_2)-TB was carried out, by studying dense films prepared from either dichloromethane or chloroform using thermogravimetric analysis and gas permeation. Molecular models of the PIM-EA(H_2)-TB polymer were also developed, taking into account the presence of residual solvent molecules within the polymeric matrix. Recent improvements in the computational field enable understanding of complex molecules and polymeric systems via superior methods such as molecular mechanics and dynamics. Molecular dynamics (MD) has a good record of predicting the fractional free volume (FFV), fractional accessible volume and cavity size distribution of membranes that are in good agreement with experimental data [23–27] and in estimating the solubility parameters of polymers and dyes [28, 29].

MD simulations investigated the gas solubility as well as the morphology of the free volume of the dense PIM-EA(H_2)-TB films with or without residual solvent, theoretically proving the effect of the casting solvent on their gas transport properties. Based on results from the combined experimental and computational studies, composite membranes were prepared from PIM-EA(H_2)-TB solutions using dichloromethane as the preferred solvent. Commercially available supports were used for the flat-sheet membranes, while porous PAN–based hollow fibres were spun *ad hoc* and then coated. The effect of coating conditions on the permeation properties of the composite membranes was studied. An important issue is the adhesion between the selective layer and the support, which depends on both chemical and physical interactions occurring at the interface and seems particularly relevant in the case of rigid polymers. Furthermore, the films obtained by controlled solvent evaporation undergo residual stresses after their formation, causing a further risk of delamination from the support. In order to improve the adhesion between the supports and the selective layers, the PAN-based hollow fibres were hydrolysed, partially converting the cyano groups into carboxyl groups and an optimization of the coating conditions was carried out to produce dense selective layers.

EXPERIMENTAL SECTION

2.1. Materials

Dichloromethane (DCM), chloroform ($CHCl_3$) and *n*-hexane, purchased from VWR, Italy, were used for the preparation of the PIM solutions. Polyacrylonitrile (PAN), containing 6 wt.% of vinyl acetate comonomer and supplied by Montefibre SpA, Italy, was used for the spinning of porous hollow fibres (HFs). Polyvinylpyrrolidone (PVP) and dimethylformamide (DMF), used as additive and solvent for PAN, were purchased by BASF, Germany and Sigma–Aldrich, Italy, respectively. Commercially available reagents were used without further purification.

The silicone elastomer Sylgard® 184 (Dow Corning), dissolved in *n*-hexane, was used for creating a smooth additional layer inside of the hollow fibres. A two-component epoxy resin (Stycast 1266, Emerson and Cuming, Belgium) was used for potting the hollow fibres in the modules for testing with gases. Nitrogen, oxygen, methane, helium, hydrogen and carbon dioxide (all with a purity of 99.99+%) were supplied by SAPIO, Italy.

2.1.1. PIM-EA(H_2)-TB synthesis

Under a nitrogen atmosphere, 9,10-dihydro-2,6(7)-diamino-9,10-ethanoanthracene (3.00 g, 13 mmol) was dissolved in dimethoxymethane (4.83 g, 63 mmol) and the solution cooled in an ice bath. Trifluoroacetic acid (25 ml) was added drop-wise over 30 min and the mixture was stirred for 24 h at room temperature. The viscous orange mixture was slowly poured into aqueous ammonium hydroxide solution and stirred vigorously for 2 h during which a white solid was formed. The solid was collected by filtration, washed with water and then acetone until the washings were clear. The resulting white powder was dissolved in chloroform (50 ml) and methanol was added drop-wise until the solution became turbid. The solution was stirred for a further 30 min to precipitate a gel. The re-precipitation from chloroform was repeated twice. The crude polymer was dissolved in chloroform (50 ml) and added drop-wise to *n*-hexane (400 ml) with vigorous stirring and the precipitated fine powder was filtered. The white powder was refluxed in methanol for 24 h, filtered and then dried in a vacuum oven for 9 h to afford desired polymer (3.15 g, 91%) as a white powder. ^{1}H NMR (500 MHz, $CDCl_3$) δ 6.84 (br, m, 4H), 4.60 (br, s, 2H), 4.05 (br, s, 4H), 1.56 (s, br, 6H). ^{13}C NMR (100 MHz, solid state) δ_C 146.5 (br), 143.3 (br), 140.2 (br), 125.1 (br), 120.6 (br), 68.1 (br), 59.7 (br), 44.9 (br), 27.5 (br); GPC (chloroform): M_n = 9,300, M_w = 49,500. BET surface area = 845 m^2 g^{-1}; total pore volume = 0.62 cm^3 g^{-1} at (P/P_0 = 0.98); TGA analysis: Initial weight loss due to thermal degradation commences at ~ 260 °C with a 10% loss of mass below 400 °C consistent with the loss

of an ethylene fragment from the ethanoanthracene unit via a retro Diels-Alder reaction and a further 24% mass loss below 1000 °C.

The molecular structure of PIM-EA(H_2)-TB is shown in Figure 1, with that of the Tröger's base and of the PIM-EA-TB polymer.

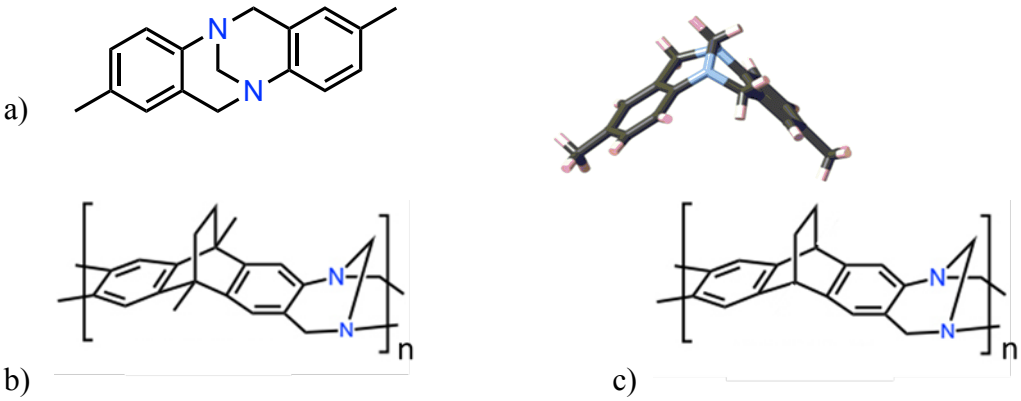

Figure 1. The structure of (a) Tröger's base; (b) PIM-EA-TB and (c) PIM-EA(H_2)-TB.

2.2. Membrane preparation

2.2.1 Isotropic dense reference films

Dense isotropic films were prepared by solvent evaporation, starting from a 5 wt.% solution of PIM-EA(H_2)-TB in DCM or from a 3 wt.% solution in $CHCl_3$. The solution was poured in a stainless-steel ring put on a glass plate and the solvent was evaporated at room temperature. The evaporation rate was controlled by partially covering the casting ring. The membranes were dried in an oven at 30 °C for 4 hours.

2.2.2 Hollow fibre supports

Porous PAN HFs were prepared by the dry-jet wet process, in a pilot plant described elsewhere [30]. The prepared dope solution was kept overnight under mechanical stirring in a thermostatic vessel before spinning. The spinning conditions and the materials were based on a previous work [31] and opportunely modified as summarised in Table 1. A mixture of DMF and ultrapure water was used as the bore fluid and water as the external coagulant. The spinning tests were performed at room temperature. The fibres, cut in pieces of 30 cm, were immersed for 24 hours in deionized water to remove residual solvent and the soluble additive (PVP). Prior to their use, they were washed in baths of decreasing polarity, from water, to ethanol, *i*-propanol and *n*-hexane.

Table 1. Materials and operating conditions for the preparation of PAN-HF supports.

Dope			Bore fluid		
Composition PAN/PVP (%wt./%wt.)	**Flow rate** (g min^{-1})	**T** (°C)	**Composition H_2O/DMF** (%wt./ %wt.)	**Flow rate** (g min^{-1})	**T** (°C)
15/12	12	70	40/60	15	20

Spinneret dimensions: OD/ID = 2.0/1.0 mm; air gap = 50 cm; external coagulant at 15 °C.

2.2.3 COOH-Functionalization of the PAN-HFs

The PAN-based HFs were functionalised by (partial) hydrolysis of the nitrile to amide and carboxyl groups in order to induce a stronger interaction with the amine groups in the PIM-EA(H_2)-TB backbone. The procedure involved NaOH solutions (0.5 M or 2.0 M) at 40 °C [32]. The solution was circulated in the lumen of the fibres by means of a peristaltic pump or, alternatively, the HFs were completely immersed in it for a fixed time. The fibres were then neutralised (HCl, 2 M, 30 min) and washed with deionized water.

2.2.4 Composite membranes

Thin film composite membranes were developed by coating flat-sheet and hollow fibre supports with PIM-EA(H_2)-TB. The PIM was dissolved in dichloromethane and kept under magnetic stirring overnight at a concentration in the range 0.5-5 wt.%. The addition of small amounts of the *n*-hexane as a non-solvent (DCM/hex = 96/4 wt./wt.) was also considered to modify the polymer state in the solution.

The flat-sheet supports were PAN-based membranes with a mean pore size of ca. 20 nm (supplied by HZG, Germany) or Fluoroplast (F-42) membranes having a mean pore size of ca. 50 nm (supplied by ZAO STC "Vladipor", Russia). The same supports with an additional silicone layer were also used. Composite flat-sheet membranes were prepared by solution casting and controlled solvent evaporation. The support, fixed on a glass plate, was coated by pouring the solution while keeping the glass plate on an inclined surface for the solution draining, or by means of a doctor blade with a gap set at 100 μm. The solvent was evaporated in air.

Composite HF membranes were prepared by coating the outer surface of the above described PAN-based HFs (standard and vacuum-assisted dip-coating) or by internal dynamic coating. Both pristine and chemically treated PAN supports were used. The inner coating was performed on the fibres already fixed within a 20 cm glass module. The fibres presented an effective length of 18 cm and an effective total membrane area of about 25 cm^2. Instead, the dip-coating was carried out on specimens that were fixed in a short aluminium tube with epoxy resin and sealed at the other end. The effective

fibre length was ca. 10 cm. The typical contact time of the fibre within the polymeric solution was 30 s. The coating was carried out in ambient conditions or in controlled conditions within a box maintained at ca. 38 °C and RH < 30%.

2.3. Characterization

2.3.1 Gel Permeation Chromatography (GPC)

Gel Permeation Chromatography was carried out using a Viscotek GPC Max1000 system which includes a refractive index detector and two 2 columns (KF-805L Shodex). The analysis used dilute solution of polymer in chloroform (1 mL min^{-1}). The analysis revealed a molecular weight (M_w) of ~49,500 g mol^{-1} (M_w), with PDI = 5.3.

2.3.2 Thermogravimetric Analysis (TGA)

The TGA was performed using the device Thermal Analysis SDT Q600 at a heating rate of 10 °C min^{-1} from room temperature to 1000 °C. TGA analyses were performed to determine the amount of residual solvent trapped in the films. Membrane samples (6-8 mg) were tested after different conditioning steps, reproducing those used before the membrane permeability tests.

The film (650 mg in 15 ml of solvent) was cast from DCM or $CHCl_3$. Solvent was evaporated for 72/96 hours in the case of $CHCl_3$, only 24/36 hours for DCM.

The film was soaked in methanol for ca. 8 hours and then the methanol was changed with a fresh quantity and left overnight. The day after the methanol was removed from the Petrie dish and the film was left to dry at room temperature for one week. The film was dried under a gentle flow of nitrogen overnight. Finally, it was put under vacuum at 25 °C for 8 h.

2.3.3 IR spectroscopy

Infrared analyses were performed by using a FT-IR spectrophotometer (Spectrum One, Perkin Elmer) equipped with the attenuated total reflection device (ATR) for direct examination of hollow fibre samples before and after their functionalization.

2.3.4 Morphological Analysis

The morphology of the composite membranes was observed by scanning electron microscopy (SEM). Sample specimens were freeze-fractured in liquid nitrogen to guarantee a sharp fracture, and, after sputtering with gold, were observed using an EVO|MA 10 (Zeiss, Italy). The thickness of the coating layer in composite membranes was evaluated from the SEM image of the cross section.

2.3.5 Gas permeation tests

The transport properties of permanent gases were evaluated for the supports, the PIM-EA(H_2)-TB isotropic films and for the composite membranes. Permeation rate measurements were performed in a fixed volume/pressure increase instrument (EESR, Germany) at 25 °C and at a feed gas pressure of 1 bar. The permeate side was kept under vacuum by a sequence of stage pumps, with a final turbomolecular pump. Details of the instrument and the method are described elsewhere [S.C. Fraga, M. Monteleone, M. Lanč, E. Esposito, A. Fuoco, L. Giorno, K. Pilnáček, K. Friess, M. Carta, N.B. McKeown, P. Izák, Z. Petrusová, J.G. Crespo, C. Brazinha, J.C. Jansen, A novel time lag method for the analysis of mixed gas diffusion in polymeric membranes by on-line mass spectrometry: Method development and validation, J. Memb. Sci. 561 (2018) 39–58. doi:10.1016/J.MEMSCI.2018.04.029.]. Before analysis, the membrane samples were carefully evacuated to remove previously absorbed species.

The gas permeance (P/l), the ratio of the permeability (P) to the membrane thickness (l), was calculated from the slope of the time-pressure curve in steady state condition:

$$p_t = p_0 + \left(dp/dt\right)_0 \cdot t + \frac{RT \cdot A}{V_P \cdot V_m} \cdot \frac{p_f \cdot P}{l} \cdot t \qquad (1)$$

where p_t is the permeate pressure at time t, p_0 the starting pressure, $(dp/dt)_0$ the baseline slope, R the universal gas constant, T the absolute temperature, A the effective membrane area, V_P the permeate volume, V_m the molar volume of a gas at standard conditions (0 °C and 1 atm), p_f the feed pressure and l the membrane thickness.

The thickness of the isotropic dense films was determined by a multiple-point measurement, using a digital micrometer (Mitutoyo, model IP65) and used to calculate the permeability from the permeance. The data elaboration, according to the time-lag method, provided the gas diffusion coefficient (D) [33]. The solubility of the gas (S) in the polymer matrix was indirectly calculated assuming the validity of the solution-diffusion permeation model ($P = D \cdot S$) [34].

The ideal selectivity was determined as the ratio of permeance of two gases and used as an indicator of the quality of the composite membranes.

A membrane area of 2.14 cm^2 was used for flat-sheet membranes. In the case of the composite HF membranes, the effective membrane area was in range 2-3 cm^2.

2.4 Computational Methods

Models of PIM-EA(H_2)-TB were built using the Material Studio 7.0 (MS) package provided by BIOVIA [35]. Solubility was predicted using the Sorption module in MS modelling, diffusivity coefficients were calculated by the mean square displacements of each gas molecule in the cells simulated by molecular dynamics runs. Amorphous polymer packings were constructed using the Theodorou/Suter method [36] as implemented in the Amorphous-Cell module. The MD simulations were performed with the PCFF force field [37].

2.4.1. Construction of PIM-EA(H_2)-TB Membrane Models

A single repeat unit with assigned charge groups and subsequent energy minimization of PIM-EA(H_2)-TB was prepared. For the minimization, a standard algorithm was employed, starting with a steepest descent stage, switching to conjugate gradient when the energy derivative reaches 1000 kcal mol^{-1} $Å^{-1}$ followed by a Newton–Raphson optimisation algorithm. For the final convergence a derivative of less than 0.001 kcal mol^{-1} $Å^{-1}$ was accepted. A single atactic homopolymer with 15 repeat units (1860 atoms) was constructed using random torsional angles and rapidly optimised (500 steps).

The PIM-EA(H_2)-TB template chain for the initial packing consisted of the 15 monomers and every packing model contained five polymer chains. Accordingly, a total of 2795 atoms were grown in a 3D model under periodic boundary conditions using the method of Theodorou/Suter with a Monte Carlo self-avoiding walk algorithm [36] implemented in the Amorphous Cell module of the BIOVIA package [35]. Moreover, 400 randomly distributed solvent molecules were inserted as obstacles in the 3D models during the Monte Carlo chain growth stage. The solvent molecules were introduced also to avoid the artefacts of catenated rings spearings, allowing for a much more homogeneously packed chain configuration, as well as for a more uniform free volume distribution within the matrix. Thus, we prepared two set of 3D of independent packing models: two models containing DCM as solvent molecules and two with $CHCl_3$.

Temperature was set at 298 K whilst the initial density was set at about ~30% of the final density. The solvent molecules, apart the amounts determined by TGA analysis, were later removed during optimization of the structures in four steps [36, 39] (Table 2).

Table 2. Parameters used in the PIM-EA(H_2)-TB membrane models.

Solvent	MW (g mol^{-1})	Solvent Density (g cm^{-3})	T_{bp} (°C)	Molecule Surface Area ($Å^2$)	Occupied Volume ($Å^3$)	Weight loss* (wt.%)	# solvent molecules**
DCM	85	1.33	40	66.69	46.69	15	36
$CHCl_3$	119.4	1.47	61	96.16	70.45	25	43

*Experimental data from TGA

**As determined from the TGA data

After each removal the structures were relaxed, applying a scheme that includes the force field parameter-scaling [38] consisting of energy minimization and NVT (constant number of particles, volume and temperature) MD runs (of 50 ps) at 303 K combined with "scaling" of conformation energy terms and non-bonded interaction energy terms in the force field (Table 3). The removal of spacer molecules leaves higher spaces than that corresponding to the experimental density.

Table 3. Scaling of conformation energy terms and nonbonded interaction energy terms in the force field.

Stage of equilibration	Scaling factor for the conformation energy terms in the force field	Type of nonbonded interaction energy term	Scaling factor for atomic radii in the nonbonded interaction energy terms
1	0.001	Repulsive 4th order	0.5
2	0.1	Repulsive 4th order	0.5
3	1	Repulsive 4th order	1
4	1	6-9 potential + Coulomb	1

The cells were then refined by employing three temperature cycle NVT runs (annealing), with temperatures up to 600 K. NVT dynamics at 303 K were used to further relax the polymer structure. Then, the system was cooled back to 500, 400, and finally 303 K alternating energy minimizations. The duration of the NVT dynamics simulations at each temperature was of 5000 fs.

Then, to increase the density of packing models a set of NPT (constant number of particles, pressure and temperature) MD runs at pressures of 100 bars were performed.

Final equilibration was performed by a 5 ns long NPT MD run at constant temperature, pressure and number of particles. The initial velocities were randomly evaluated, setting the time step to 1 femtosecond (fs) and keeping the temperature and pressure constant, using Andersen pressure control [40]. The Atom Based method was used for controlling long-range Coulomb and van der Waals interactions. The side length of the bulk models was about 4.2 nm and the final density was 1.06 $\pm$ 0.05 g cm^{-3} for the models containing DCM as residual solvent and 1.16 $\pm$ 0.04 g cm^{-3} for models containing $CHCl_3$. These values are in agreement with the experimentally measured values of 1.01 $\pm$ 0.05 g cm^{-3} for dense films with DCM and 1.13 $\pm$ 0.09 g cm^{-3} for dense films with $CHCl_3$. It is worth stating that small deviations in obtaining the experimental density can occur for glassy stiff-chain polymer materials [42]. The simulation conditions were: a minimum image boundary condition to

make the system numerically tractable and to avoid symmetry effects and a cut-off distance of 20 Å with a switching function in the interval 18.5–20 Å. Through the dynamics, the Andersen pressure control [40] and the Berendsen temperature control method [41] were used. In the absence of experimental evidence, swelling or plasticization are not taken into account in the molecular modeling either.

2.4.2. Pair Correlation Functions: (RDF) Analysis

The radial distribution function (RDF) was adopted to analyse the microstructure of the material. The pair correlation functions $g_{AB}(r)$ [43] were used for evaluating the relative positions of selected atoms, molecules or chemical groups in our systems at microscopic scale. $g_{AB}(r)$ represents the probability of finding a pair of particles *AB* at a distance *r(dr)* normalised to the probability expected for a completely random distribution at the same density:

$$g_{AB}(r) = \frac{V\left\langle \sum_{i \neq j} \delta(r - |r_{Ai} - r_{Bj}|) \right\rangle}{(N_A N_B - N_{AB}) 4\pi r^2 \, dr} \tag{2}$$

where *A* and *B* are two kinds of particles. The system has a volume *V* and contains N_A particles of kind *A* and N_B particles of kind *B,* with N_{AB} particles belonging simultaneously to both kinds. Vectors r_{Ai} and r_{Bj} represent the position of particle *i* of kind *A* and particle *j* of kind *B*, so that $|r_{Ai} - r_{Bj}|$ is the distance between those two particles. The term $\delta\left(r - |r_{Ai} - r_{Bj}|\right)$ is set to unity when $\left(r - |r_{Ai} - r_{Bj}|\right) \leq$ *dr* (*i.e.*, the difference between the desired and the actual distance between the two particles is smaller than a tolerance factor *dr*) and to zero otherwise.

2.4.3 Calculation of Solubility Coefficients

The Sorption module of the software was used to simulate sorption of CO_2, O_2, N_2 and CH_4. The calculations were carried out in the Grand Canonical Monte Carlo (GCMC) ensemble at fixed temperature, volume, and chemical potential using the Metropolis Algorithm [44, 45] and with the PCFF force field [37]. MC simulation can be done by physically and unnatural trial moves. These trial moves happen according to the system requirements which are: rotation, displacement, translation and regrowth. The Metropolis algorithm was used to accept or reject an insertion and deletion of a sorbate molecule The probability of addition and deletion of a sorbate molecule is:

$$P_{add} = \min\left[1; \frac{1}{N_s + 1} \frac{pV}{k_b T} \exp\left(\frac{-\Delta U}{k_b T}\right)\right] \text{ and } P_{del} = \min\left[1; \frac{N_s k_b T}{pV} \exp\left(\frac{-\Delta U}{k_b T}\right)\right] \quad (3)$$

where U is calculated from the sum of non-bonded (*i.e.*, Coulombic and van der Waals interaction) energies and N_s is the number of sorbate molecules. The addition is accepted if the energy change ΔU is negative or if the Boltzmann factor is greater than a random number generated between 0 and 1. Single gas isotherms were calculated in the range between 0 and 5 bar. The solubility coefficient S was calculated from the number of gas molecules loaded into the polymer 3D model under 1 bar and 25 °C conditions, to compare with the experimental data obtained under the same conditions. Referring to GCMC Simulations: at each pressure, 10^6 steps of GCMC calculations were performed using an initial equilibration period of 5000 steps. The charge interaction was considered and the non-bond cut-off was set to 12 Å. Loading was performed into models that were built with a percentages of 1) DCM of 15 %wt. (i.e. 36 molecules) and 2) $CHCl_3$ of 25 %wt. (i.e. 43 molecules) in addition to the PIM-EA(H_2)-TB polymeric chains.

2.4.4 Accessible Free Volume and Fractional Free Volume

A free volume analysis was carried out using the Visualizer module of the BIOVIA software package [35]. First, the van der Waals surface was defined as the surface that intersects with the vdW radii of the atoms in the given structure, where the volume on the atom side of the surface (occupied volume) is used as the van der Waals volume. Based on the van der Waals surface, the accessible solvent surface was also defined as the locus of the probe centre as the probe rolls over the scaled vdW surface. This surface describes a space, which could, in principle, be occupied by a probe of the given radius and is only defined over externally accessible regions, where the volume on the side of the surface without atoms (the free volume) is used as the accessible free volume.

The FFV is the ratio of the free volume, V_f, of a polymer (cm^3/g) and the specific volume, V_{sp}, defined as reciprocal density:

$$FFV = \frac{V_f}{V_{sp}} \quad (4)$$

According to the Bondi method [46], the free volume can be estimated as:

$$V_f = V_{sp} - 1.3V_{vdW} \quad (5)$$

where the van der Waals volume V_{vdW} is calculated using a group contribution method, and a universal "packing coefficient", equal to 1.3, is used to convert the van der Waals volume of the repeat unit into the "occupied" volume.

3. Results and discussion

3.1 Isotropic dense films

The dense films of PIM-EA(H_2)-TB were used to obtain the intrinsic values of permeability and selectivity and assumed as reference values for the composite membranes. The films made from the same polymer batch, dissolved in DCM or in $CHCl_3$, presented some differences. The film cast in DCM shrunk much more than the chloroform one and, just after casting, it looked more flexible and robust. This could be due to the faster evaporation, as the DCM film was ready after ca. 24 h because of the lower boiling point of the solvent, whereas for the $CHCl_3$ at least three days were required.

The role of the solvent, used for casting the films based on PIM-EA(H_2)-TB, was experimentally evaluated by TGA and permeation tests and theoretically investigated with MD simulations.

Two PIM-EA(H_2)-TB films, prepared using $CHCl_3$ or DCM and left ca. 3 days to dry, were analysed using TGA (Figure 2 and Figure S1). A significant presence of residual solvent, was found if compared to the range for polyimides (ca. 1 wt.% of DCM or NMP in 6FDA–*m*PDA [47]). The film cast using DCM retained a lower amount of solvent (ca. 15 wt.%), while the film cast from $CHCl_3$ showed a remarkable 25 wt.% of residual solvent (Figure 2a). This could be due to the higher polarity of chloroform, which is kept more tightly into the PIM-film and to its slightly higher acidity that helps to bind more tightly to the basic TB tertiary amines, along with its higher boiling point compared to DCM. The total solvent removal occurred at a temperature of over 200 °C.

After methanol treatment, the two films of PIM-EA(H_2)-TB, cast in DCM or $CHCl_3$, behave in the same way and their TGAs were perfectly superimposable (Figure S1a). On substitution of DCM with methanol, the polymer dried more quickly and the solvent was released from the polymer almost violently under vacuum (and at a much lower temperature). Its rapid shrinking during this process makes it also fragile. Vacuum drying at room temperature was not able to remove all the cast $CHCl_3$, in fact ca. 22 wt.% of solvent was still present vs. the 25 wt.% present in the "air dried" sample. Only under vacuum and at 100-120 °C was the solvent (almost) completely removed.

Figure S1b shows the overlay of TGAs for the PIM-EA(H_2)-TB film cast from DCM and then treated in MeOH. The film 'as cast' presented a residue solvent of about 15 wt.%, the MeOH treated film dried under N_2 showed a reduction up to 8 wt.% and the same sample put under vacuum at 25 °C showed a further reduction of the solvent up to only 3.8 wt.%. Considering how easily methanol is removed (TGA less than 100 °C), this is likely to be due to some residual moisture. The rest of the

trapped solvent was easily removed under vacuum. The film left in open air and measured again after 1 week and 2 weeks showed only a slight increase of the solvent (Figure S1b), which is likely to be water adsorbed due to the porous nature of the polymer.

Increasing the temperature under vacuum eliminates the solvent completely. A methanol treated powdered sample (left 24 h at 120 °C under vacuum) showed that there is always a little residue of solvent (ca. 1.5-2 wt.%), again attributable to trapped solvent or moisture. It has been demonstrated previously that the solution processing necessary to form freestanding membranes of PIM-1 results in an increase in free volume when compared to the intrinsic free volume of the powder [48]. The rest of the TGA curves of PIM-EA(H_2)-TB, representing the retro Diels-Alder between 330 and 425 °C, does not change once the polymer has lost all the solvent (Figure 2).

a)

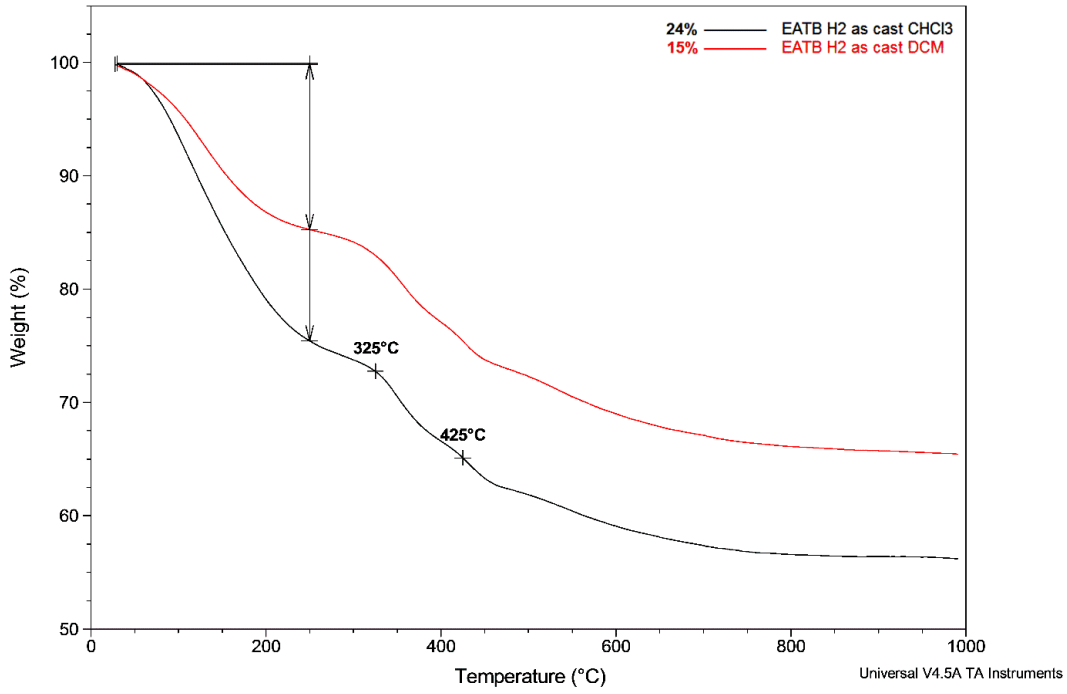

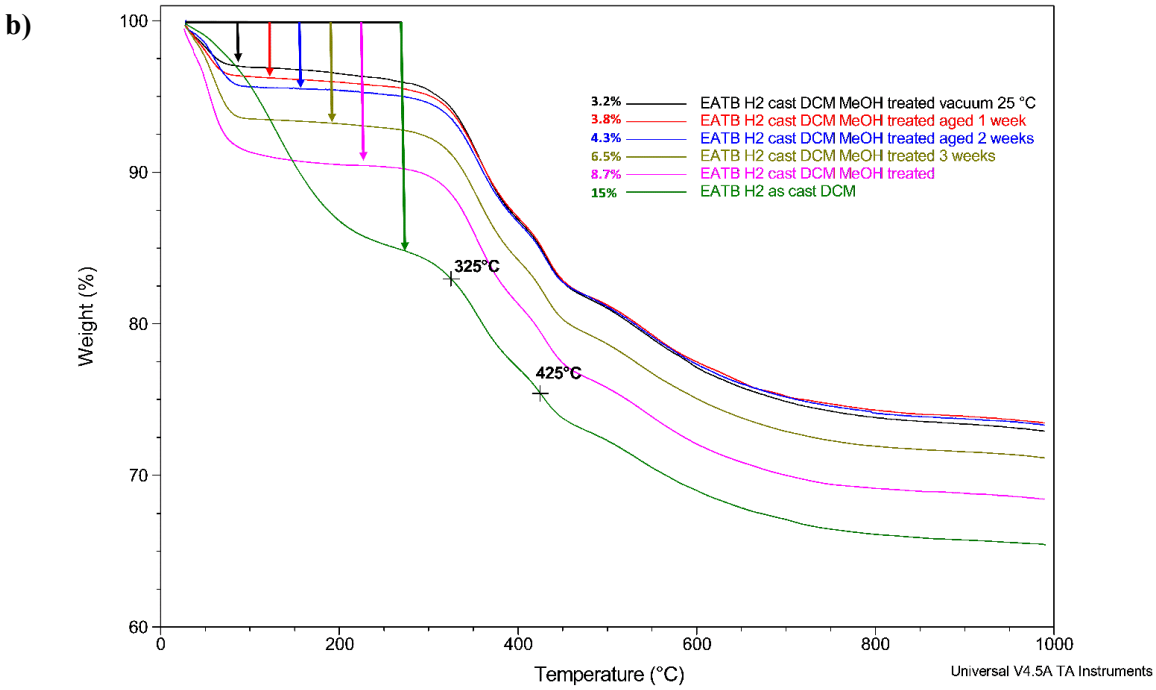

Figure 2. TGA of PIM-EA(H_2)-TB films. a) Overlay of two films cast from $CHCl_3$ or DCM; b) overlay of a film cast from DCM, MeOH-treated and aged.

The analysis of the Hildebrand Solubility Parameter (δ) of polymer and solvent molecules supported the TGA findings. This parameter is a molecular descriptor based on the cohesive energy density (CED) [49]. Materials having close solubility parameters will dissolve in each other or, at least, have a high affinity toward each other. The solubility parameters of the solvent molecules and polymer were calculated using MD simulations and a group contribution method:

$$\delta = (CED)^{\frac{1}{2}} = \left[\frac{\sum E_{cohi}}{\sum V_{mi}}\right]^{1/2} \quad (6)$$

where E_{cohi} is the cohesive energy for the i^{th} functional group of the molecule and V_{mi} is its molar volume.

The two methods yielded comparable values (Table 4), showing similar properties for the solvent molecule, thus demonstrating their mutual affinity. Consequently, we consider also the value for δ of polymer acceptable. The results indicated that both $CHCl_3$ and DCM are good solvents for PIM-EA(H_2)-TB (as for PIM-1 [50]), however, the polymer usually shows better interaction with $CHCl_3$. Moreover, $CHCl_3$ is responsible for inducing hydrogen bonding or weaker interactions, depending on the chemistry of the polymeric matrix. For example, in a PEI polymer there are three sites available for hydrogen bonding: N atoms, carbonyls of imide groups and ether bonds [17]. In PIM-EA(H_2)-TB, $CHCl_3$ could interact only with the N atoms of the Tröger's base.

Table 4. Solubility Parameters (δ (J cm^{-3})$^{0.5}$) from MD Simulations and Group Contribution Methods.

	Solubility parameter from group contribution method	**Solubility parameter from MD simulation**
PIM-EA(H_2)-TB	*n.a.*	12.78
$CHCl_3$	18.7	18.11
DCM	20.2	20.83

As cast dense films of PIM-EA(H_2)-TB presented different permeation properties when prepared from DCM or from $CHCl_3$ (Table S1), reflecting the findings of TGA analysis.

The thickness of the film could be related to the observed differences. Generally, for glassy polymers, thinner films demonstrate lower gas permeability due to the larger relative contribution of the more densely packed surface regions of the film. In the present case, this effect does not seem significant since the thinner film (cast from DCM) is the more permeable one. More likely, the observed difference in the gas permeability could be associated to the amount of residual solvent still present in the 'as cast' samples. As noted, TGA indicated that the polymer retained a larger amount of the bulkier $CHCl_3$ that could restrict gas transport.

The observation that a larger quantity of residual solvent reduces the gas permeability is similar to that described for polysulfone or poly(phenylene oxide) in the presence of certain low molecular diluents and referred to as 'antiplasticization' [51]. Instead, for perfluoropolymers (e.g., Hyflon® AD) a plasticization exerted by the residual solvent, reducing the selectivity and increasing the permeability, was reported [52]. However, PIMs are super-glassy and extremely rigid materials for which it is difficult to induce segmental motions and no glass transition could be detected as proven by thermal analyses [5]. Therefore, excluding small molecular segment motions, the difference in separation behaviour should derive from changes in free-volume (e.g., amount, hole size and size distribution).

The observed permeation rate order for various gases was also different in the two cases. The films produced from DCM presented a higher ideal selectivity, with interesting H_2/N_2 values. Indeed, it displayed a marked size-sieving behaviour, with hydrogen more permeable than carbon dioxide, as for the methyl version of the PIM-EA-TB polymer [6]. In contrast, the film cast from $CHCl_3$ presented a 'reverse-selectivity' where carbon dioxide, the most condensable species, is the most permeable, according to the preponderant role of the solubility. This permeation order ($CO_2 > H_2 > He > O_2 > CH_4 > N_2$) was observed for other PIMs (e.g., PIM-1 [22]). In particular, PIM-1 contains SBI and dioxane linkages that can bend to a considerable level, PIM-EA-TB, instead, has a more rigid structure that restrict rotation even further, resulting in a more uniform pore organization [53]. This

structure imparts high gas permeability, coupled to size discrimination between gases having slight differences in molecular dimensions, such as O_2 and N_2.

A more detailed analysis could be done considering the two contributions to permeability, namely the diffusion and the solubility coefficients (Figure 3). These parameters reflect the penetrant/polymer interaction, but they also depend on the residual solvent and, thus, on the combination polymer-solvent. The diffusion coefficient order is: He > H_2 >> O_2 > CO_2 ~ N_2 > CH_4, according to their increasing kinetic diameters, except for CO_2. Indeed, CO_2 showed a significantly large solubility, owing to a strong interaction with the polymer, which affects its mobility. As for the permeability, the diffusion coefficients were generally greater in the film obtained from DCM. The gases with a large kinetic diameter, such as N_2 and methane, showed a higher diffusion in the sample containing $CHCl_3$. Actually, their good solubility, that is again higher in the DCM film, implies a higher amount of gas molecules in the matrix with DCM, reducing their mobility. The higher is the condensability of gases, the higher is the solubility. However, the solubility of all gases proved higher for the film with DCM as casting solvent, compared to $CHCl_3$. This reflects the production of a higher amount of free volume in the case of DCM. This is in agreement with the experimental density lower for film continuing DCM (1.01 g/cm^3) than for that with $CHCl_3$ (1.13 g/cm3). Same trend was found for the simulated fractional free volume: 0.28 in PIM-EA(H_2)-TB models containing DCM and 0.24 in those containing $CHCl_3$.. The gases considered for the permeation tests have similar solubility in the two liquid solvents, just a bit larger in $CHCl_3$ [54]. Moreover, the solubility of permanent gases in DCM and $CHCl_3$ is remarkably smaller than that in PIM polymers. For these reasons, the differences in solubility values of permanent gases in PIM-EA(H_2)-TB containing residual solvents, could not be ascribed only to the contribution of gas solubility in solvents. These are better related to the polymer contribution.

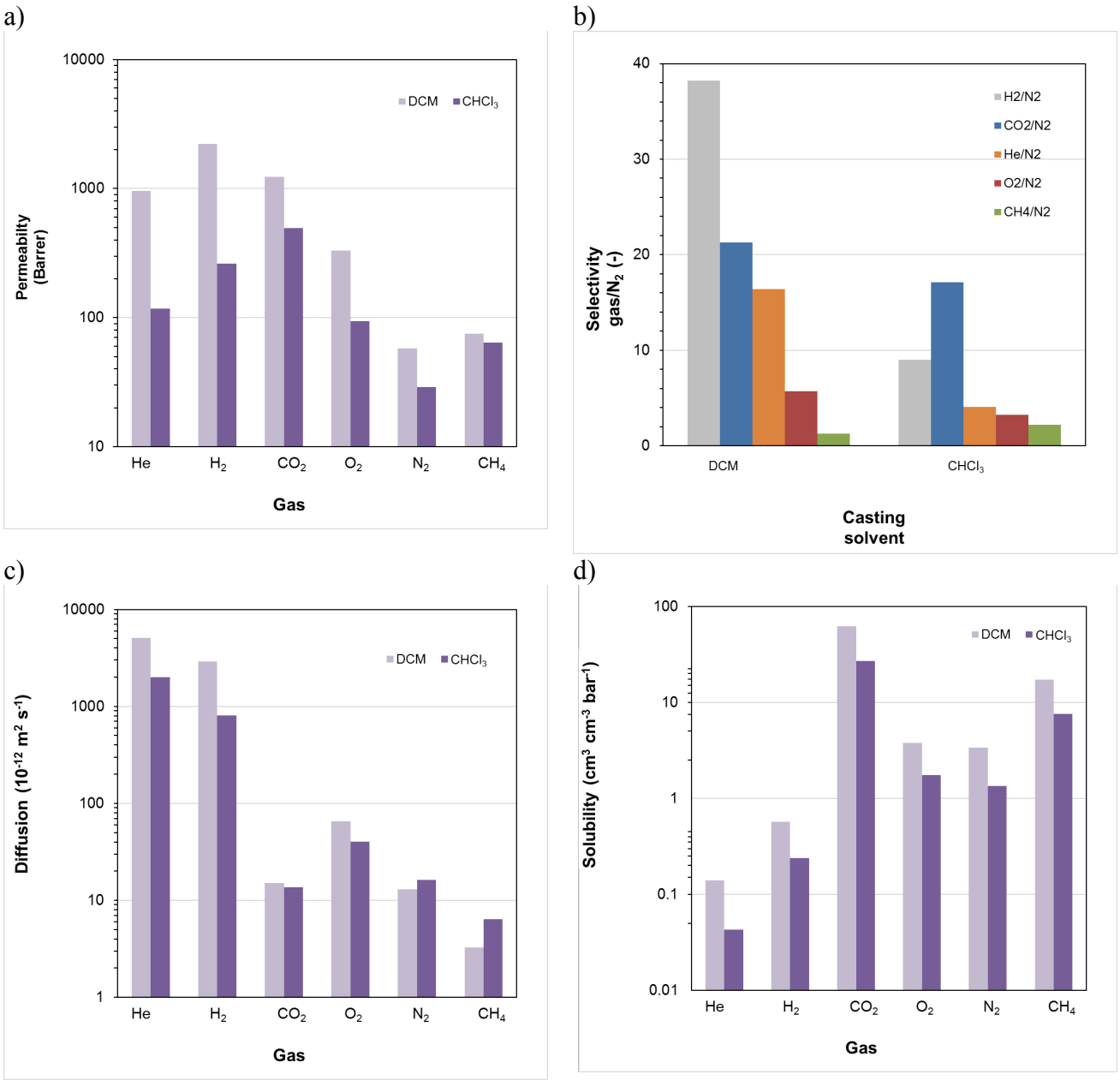

Figure 3. Permeability (a), ideal selectivity (b), diffusion (c) and solubility (d) of different gases in films of PIM-EA(H_2)-TB cast from DCM or $CHCl_3$. Gases are in the order of their relative size (kinetic diameter [55]).

To validate the constructed models, the calculated solubility coefficients of gases were compared with experimental data, showing a reasonable agreement (Figure 4). However, several effects have to be considered for gas solubility coefficient calculations. First, the framework of the adsorbent is typically fixed for simplicity. This is warranted to some degree due to the topological complexity of dense amorphous microporous polymers. This assumption is only reasonable at low pressures as in the case considered in this paper of the, due to adsorbent induced changes in the host matrix. For polymeric systems, the validity of this assumption depends on the polymer rigidity and its thermodynamic state. Current MC techniques are not adequate to address polymer relaxation in these

last cases. Moreover, the accuracy of the predictions of the *S* values is not very precise due to their crucial sensitivity to many factors such as appropriate choice of the force field, the most crucial aspect, the dimension of system model, etc., as Yampolskii [56] and other authors stated [24,57]. It can be assumed that realistic assessment of the accuracy of the *S* values for small penetrants based on contemporary GCMC simulations corresponds to a factor 3 as compared with the experimental values, which also show some scatter.

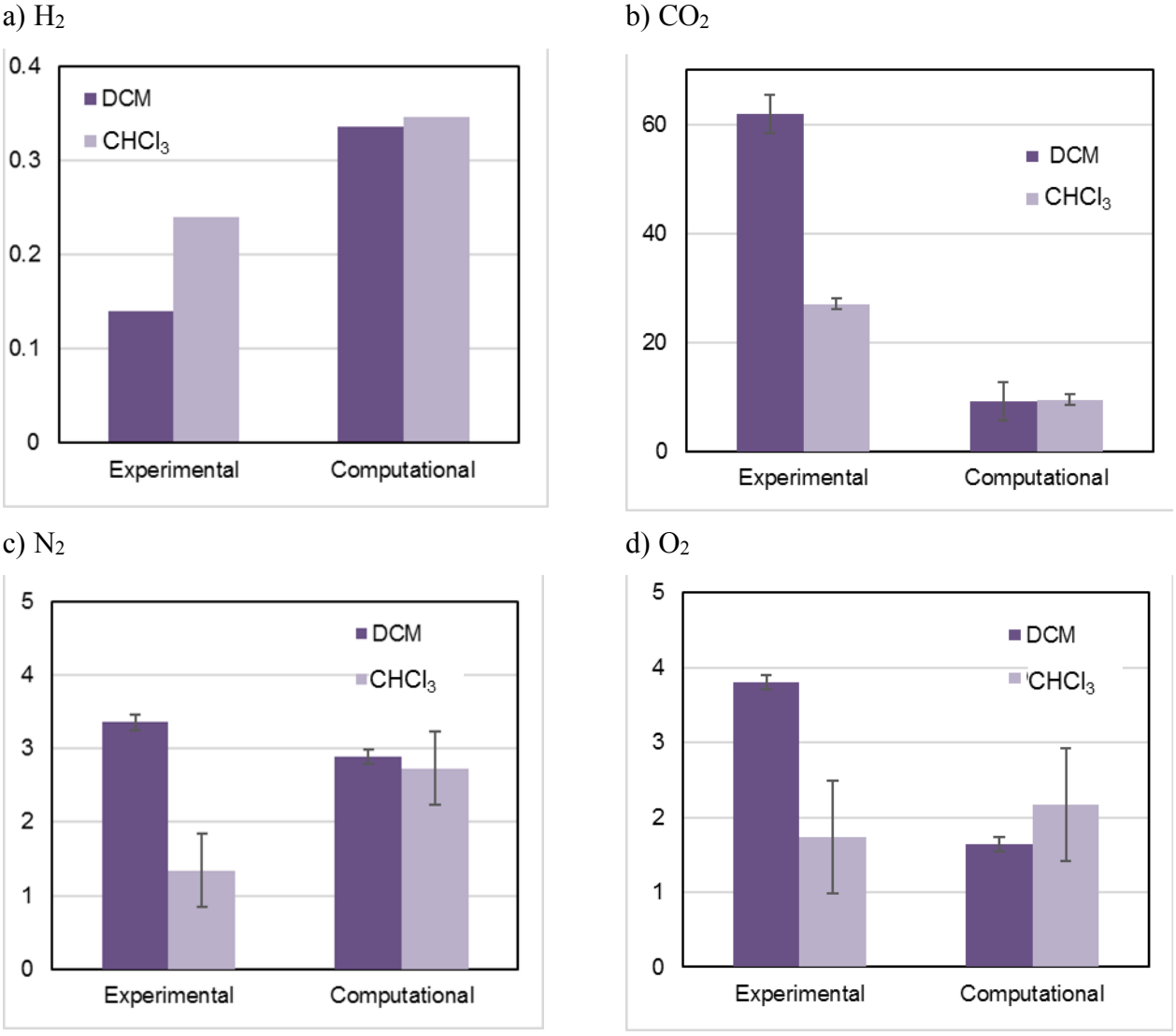

Figure 4. Gas solubility coefficients (cm^3 (STP) cm^{-3} polymer·bar^{-1}) in PIM-EA(H_2)-TB films cast from DCM or $CHCl_3$. a) H_2, b) CO_2, c) N_2 and d) O_2. Experimental *vs*. computational values.

The effect of the residual solvent, in the considered temperature of simulation, affect adsorption, however the movement of solvent molecules is less evident than the competition of gases to occupy sorption sites. Additionally, the "well-known" deviation for CO_2 is due to anisotropy and to the missing "relaxational" motions of the matrix [7]. Considering all these effects, our simulation results can be considered in an acceptable range for further discussion in this paper. This is evident when

checking the different order of gas solubilities: while the experimental solubility of N_2 is lower than that of O_2 for both membranes, the computational value of O_2 is smaller than that of N_2.

Gas solubility coefficients are larger in the film containing DCM (15 wt.%), that is present in a lower amount than $CHCl_3$ (25 wt.%), as shown by TGA. This is due to a competition to occupy sorption sites in the matrix between gas molecules and residual solvent that is reduced in the film containing less solvent molecules. Dichloromethane, having a lower boiling point than $CHCl_3$, tends to evaporate quickly during the film formation, thus occupying sorption sites to a lesser extent. Instead, the bulkier $CHCl_3$ occupies a larger fraction of available volume within the matrix, leading to a reduced gas sorption.

A fundamental contribution to the transport of CO_2 in PIMs and in PIM-EA(H_2)-TB is given by the CO_2 solubility coefficient that reflects the interaction between the gas and the polymer matrix, but it also depends on the type of residual solvent. This was confirmed investigating the associations between CO_2 and possible sites of interactions of the polymeric chains or solvent. The calculated RDF functions, averaged over all atom pairs, showed the interactions between the oxygen atom of CO_2 and the nitrogen atom of the polymer's TB group in both systems (Figure 5a) and the association between CO_2 and solvent molecules in the polymeric films (Figure 5b).

Generally, the peaks observed at less than 4 Å are assigned to a specific distance of the closely coupled atoms. At long distances, RDF approaches unity, which is quite probable for a purely amorphous system. CO_2 is associated almost at the same extent with the polymer matrix, independently on the retained solvent, with a slightly larger preference in the case of $CHCl_3$. Therefore, with the same "degree" of interaction with the matrix, the higher CO_2 solubility in the film cast from DCM depends on the higher free available space for the CO_2 molecules. The association of CO_2 with the solvent molecules in the polymer matrix is stronger with DCM than with $CHCl_3$. These two effects sum up and explain the higher CO_2 solubility in films containing DCM as residual solvent (62 (cm^3 cm^{-3} bar^{-1}) in DCM *vs* 27.1 (cm^3 cm^{-3} bar^{-1}) in $CHCl_3$).

a)

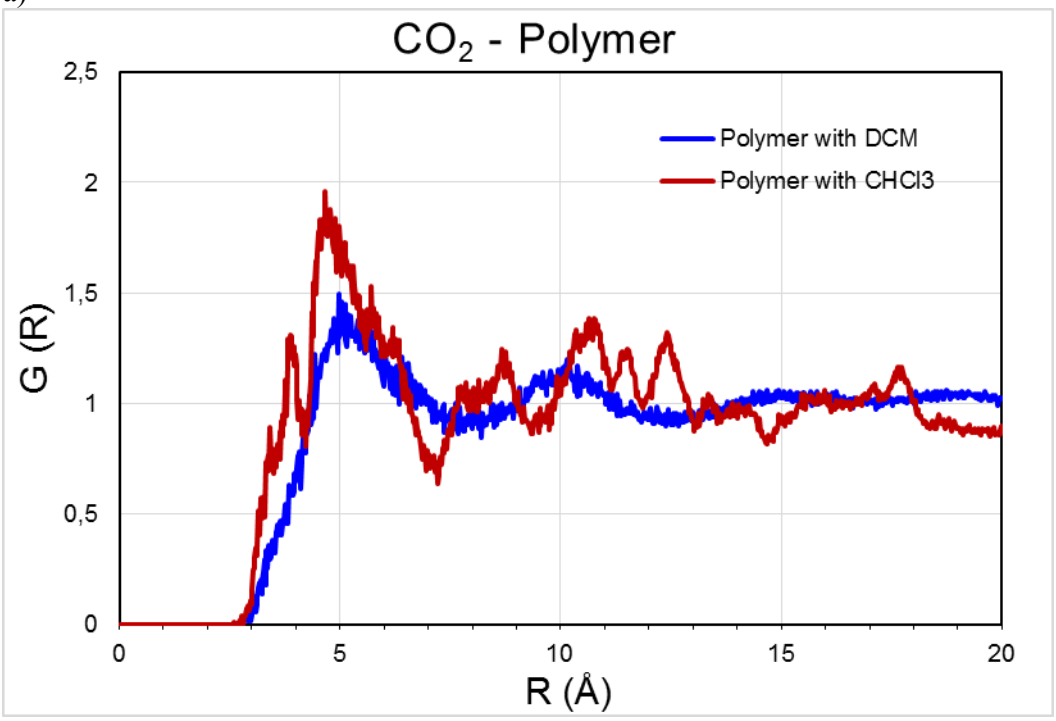

b)

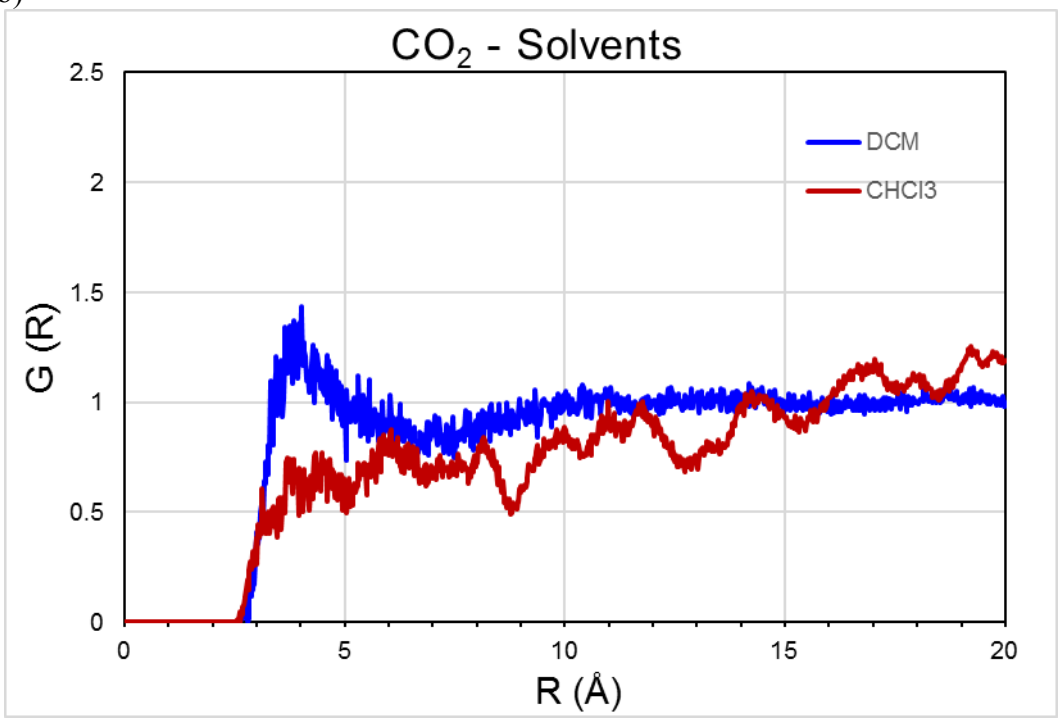

Figure 5. Radial distribution functions (RDF) between CO_2 molecule and a) the N atom of the polymer's TB group in presence of DCM or $CHCl_3$, b) Cl atoms of DCM or $CHCl_3$ in both membranes.

The diverse gas transport parameters of the PIM-EA(H_2)-TB samples cast from the two solvents clearly indicated important differences in their free volume (FV). The residual solvent molecules occupied several free spaces in the polymer matrix and the effective FV was controlled by the quantity, but also by the type of the solvent, as confirmed by molecular modelling of the organization

of the FV elements, considering the empty matrix or that with solvent molecules. Hard spherical particles, with radius ranging from 1 to 2 Å, were used to probe the 'accessible' free volume (Figure 6). 'Accessible' means that isolated free volume elements were excluded. Films containing the two solvents showed a similar behaviour: the accessible FV decreased with increasing probe radius, suggesting that the size of the FV with larger radii are reduced in number and that larger gas molecules have less space to transport through and lower diffusivity. The bulkier $CHCl_3$ molecules had lower accessible FV throughout the entire range of probe radii, while DCM, smaller in dimension and in lower concentration into the membrane matrix, left a higher amount of accessible free volume to the entire range of gas molecules. The ratio of 'accessible' free volume to its surface area (*V*/*S*) in membranes with solvent molecules was also analysed, focusing on the gas kinetic diameter. *V*/*S* is a 'shape factor' that provides the variations in the contour of the free volume. A higher *V*/*S* ratio indicates a higher volume and/or a smaller surface. The greater amount of $CHCl_3$ molecules with a larger surface area than DCM induced a total reduction in the *V*/*S* ratio and their difference became larger with increasing the probe radius (Figure 6). This implies that diffusion coefficients of H_2 and He are much greater than those of N_2 and methane, as observed in experimental data reported in Figure 3c.

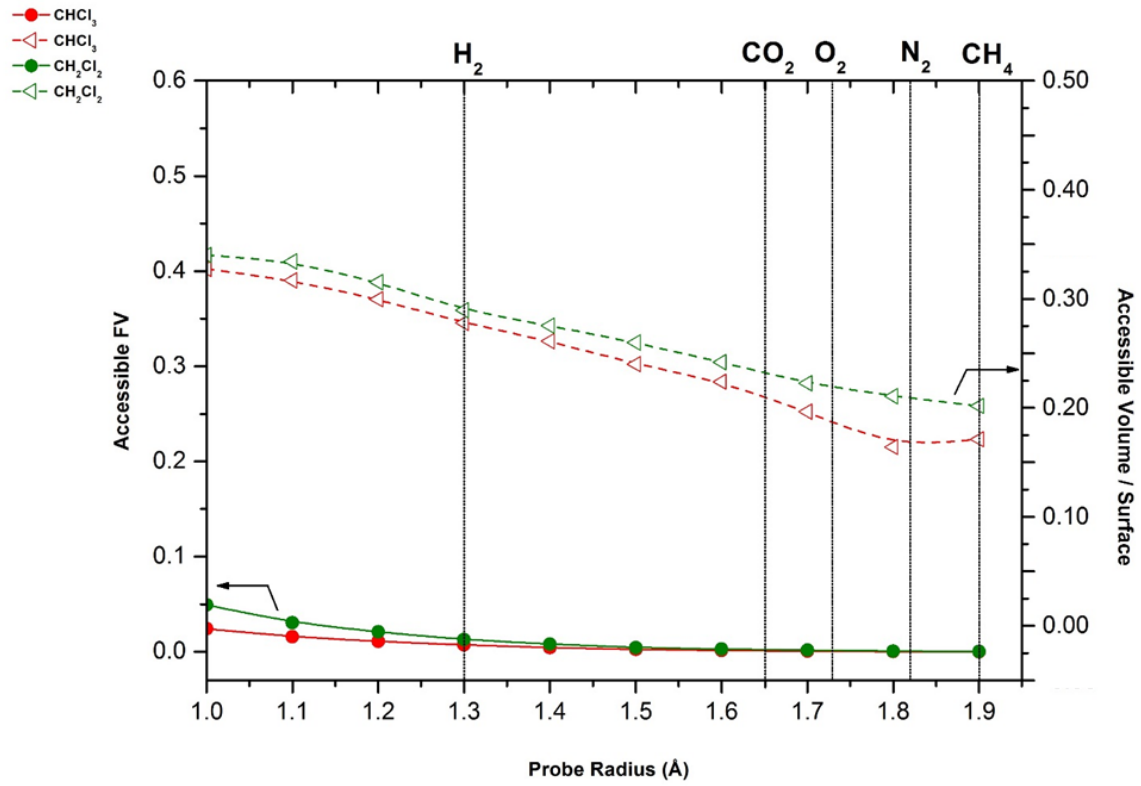

Figure 6. Accessible free volume and *V*/*S* ratio of PIM-EA(H_2)-TB membranes containing $CHCl_3$ or DCM for different probes. The dimension of H_2, CO_2, N_2 and O_2 have also been indicated (kinetic radius of H_2, CO_2, O_2 and N_2 = 1.44 Å, 1.65 Å, 1.73 Å and 1.82 Å, respectively [55]).

The amount of FV alone does not provide information on the connectivity and tortuosity of the pores, which are important for describing size-sieving effects. The FV morphology, in terms of the size, shape, size distribution and interconnectivity, has a dramatic effect on the membrane properties. Figure 7 showed the accessible free volume for different gaseous probes (e.g., H_2, N_2 and CH_4) in films that are in different states. The first 3D models refer to the "solvent-free" state and the others to the membranes with residual solvent. In all models, H_2 can access to more FV than the larger N_2 or CH_4 molecules. In addition, the accessible FV for H_2 was more interconnected than for the other probes, explaining the higher diffusivity found experimentally for H_2, as compared to N_2 (Figure 7). A greater FV was evidenced in membranes retaining DCM with respect to those containing $CHCl_3$ molecules, supporting the higher gas permeability measured in the samples prepared from DCM.

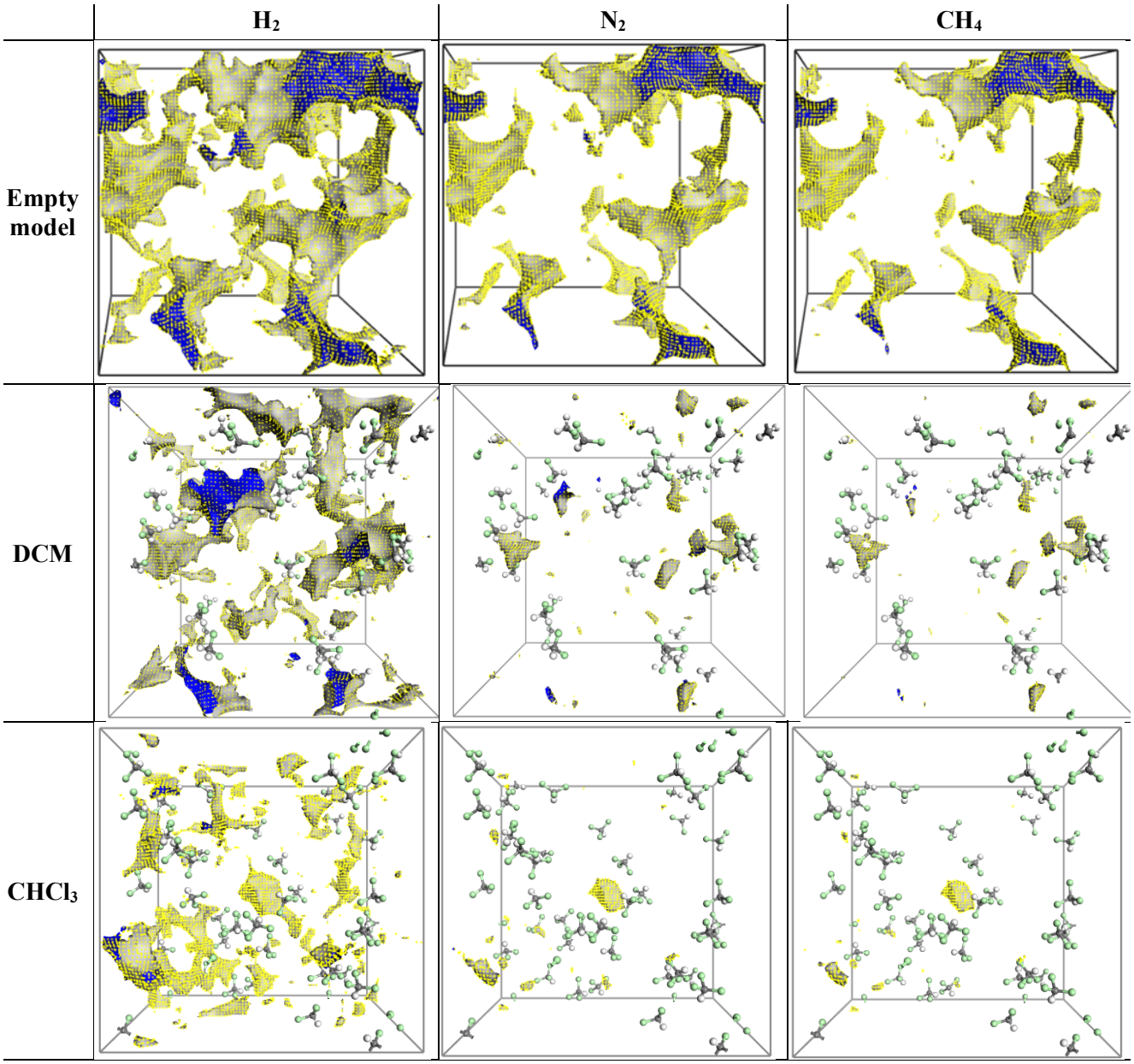

Figure 7. 3D models of the accessible free volume distribution in PIM-EA(H_2)-TB for H_2, N_2 and CH_4. Rows: empty membrane (without solvent molecules), membrane with dichloromethane and membrane with chloroform.

The investigation on the free volume elements gave valuable insights into the influence of the casting solvent on the microstructure of this polymer. The proposed molecular modelling provided a theoretical support to the observed transport properties.

3.2 Composite membranes

DCM was chosen as solvent for PIM-EA(H_2)-TB in the preparation of composite membranes on the basis of to the information from TGA and permeation tests and considering its good volatility and compatibility with the used supports. Both flat-sheet and hollow fibre supports were used for coating.

3.2.1 Supports

The Fluoroplast (F-42) flat-sheet supports presented a greater gas permeance than those based on PAN, reflecting the larger nominal mean pore size. The presence of a silicone additional layer reduced the permeance of both types of membranes (Table 5).

Table 5. N_2 Permeance of the flat-sheet supports.

Support	**N_2 Permeance**	
	(m^3(STP) m^{-2} h^{-1} bar^{-1})	(GPU)
F-42 (mean pore size of ca. 50 nm**)**	130	47500
F-42 + intermediate layer based on silicone organic block co-polymer **porous layer**	18	6600
PAN (mean pore size of ca. 20 nm)	71	26000
PAN + PDMS gutter layer	3.1	1100

1 GPU = 10^{-6} cm^3 (STP) cm^{-2} s^{-1} $cmHg^{-1}$

The prepared PAN-based HF supports showed an asymmetric porous structure with finger-like and sponge-like zones (Figure 8). The permeance of the bare supports was 80 (m^3(STP) m^{-2} h^{-1} bar^{-1}) for N_2 and 200 (m^3(STP) m^{-2} h^{-1} bar^{-1}) for He.

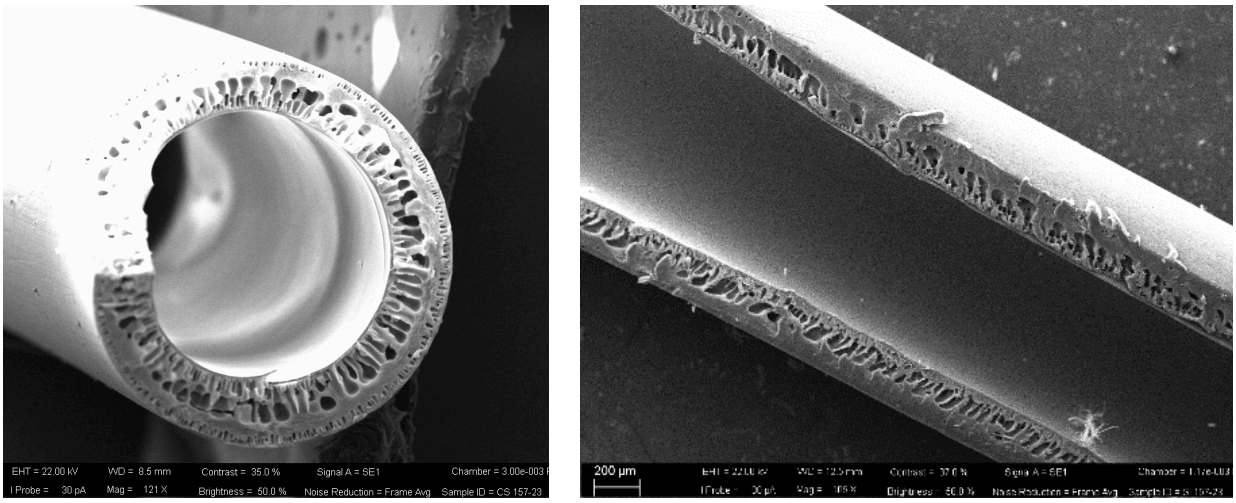

Figure 8. SEM images of the cross section of the porous PAN-based HFs.

IR spectra taken on the PAN-HFs, before and after their treatment with NaOH solutions of different concentration and for different times, are displayed in Figure 9. The broad adsorption band (around 3400 cm–1) of the active hydrogen of the hydrolysed PAN-COOH gradually increased. A prolonged treatment (24 hours) with NaOH 2 M resulted in a complete hydrolysis of the –CN group to –COOH and $–CONH_2$. The main evidence was the disappearance of the nitrile group peak at 2243 cm^{-1} and the appearance of the peaks at 1660 cm^{-1} and 1710 cm^{-1} representative of the C=O stretching of the amide and carboxyl groups, respectively. Under milder conditions (NaOH 0.5 M or 2 M, up to 2 hours), the preferred reaction was the formation of $–CONH_2$, proved by the progressive increase of the band at 1660 cm^{-1}. The ester group of the vinyl acetate portion of the copolymer was also involved in the hydrolysis, as shown by the progressive attenuation of the band at 1735 cm^{-1}, accounting for the C=O stretching of the ester group. The interactions between the –COOH groups in the hydrolysed PAN-supports with the nitrogen atoms of the TB-based PIM are expected to play a role in improving the adhesion of the support with the coating layer.

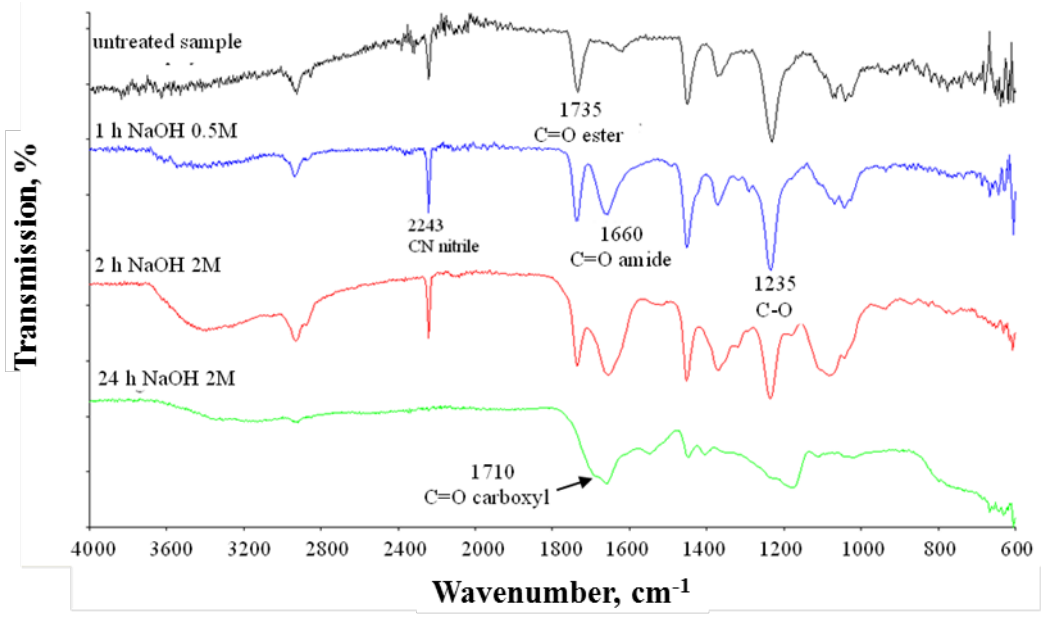

Figure 9. IR spectra of the PAN hollow fibres before and after the hydrolysis.

The hydrolysis reduced the gas permeance of the PAN-HFs, indicating a denser structure for the COOH–functionalised PAN HFs. Milder reaction conditions (NaOH 0.5 M, 1 h) resulted in a permeance loss of ca. 15–20%, while a stronger treatment (NaOH 2 M, 24 h) caused a permeance reduction of ca. 98%. To avoid the disadvantageous modifications occurring at longer NaOH treatment times, a reaction time of 1 h with NaOH 0.5 M was adopted.

3.2.2. Flat sheet composite membranes

The results of the permeation tests carried out on these composite samples for the CO_2/N_2 and H_2/N_2 gas pairs are reported in Table 6. Defect-free membranes were obtained by coating the supports comprising the intermediate silicone layer. Interestingly, the ideal gas selectivity values measured in the defect-free membranes for some gas pairs (CO_2/N_2, O_2/N_2 and particularly H_2/N_2 and He/N_2) exceeded those measured for a thick dense film (80 micron) cast by using DCM. This effect seems to be related to an accelerated physical aging in thin films of glassy polymers [48, 58]. In addition, when preparing thicker samples (dense films), different evaporation conditions are established within the membrane section that lead to a less tightly packed polymer in the bulk. A sample prepared on the (PAN + PDMS layer) support showed a reduction in permeance and an increased selectivity over time, as usually due to physical ageing [59, 60]. However, the membranes prepared on the (F-42 + silicone layer) support become less selective upon ageing. This evidenced the formation of defects, which can be due to some stresses on the coating layer connected to the polymer relaxation.

A single coating on the supports without a 'gutter' layer was not sufficient to reach the intrinsic selectivity of the PIM and a contribution of the porous support was found. The membranes prepared on PAN-based supports (mean pore size of 20 nm) had a selectivity that is half the intrinsic one. Instead, those obtained by coating F-42 supports, that presented a larger mean pore size (50 nm), showed a Knudsen-like diffusion ($CO_2<N_2$).

Table 6. Transport properties of the flat-sheet PIM-EA(H_2)-TB composite membranes (25 °C).

Coating/Polymer conc. (wt.%)	**Support**	**Permeance_CO_2** (GPU)	**CO_2/N_2** (-)	**H_2/N_2** (-)	**Testing time,** after the membrane casting
5	None, dense	1240 Barrer	21.3	38.2	'as cast'
Pouring / 5	PAN (20 nm)	77	10.1	19.2	1 d
Pouring / 3	PAN + PDMS	88	21.0	47.0	1 d
		36	26.5	61.2	40 h
Pouring / 3	PAN + PDMS	26	21.5	68.3	12 d (test at 35 °C)
Pouring / 3	PAN + PDMS	44	26.5	79.4	1 month
Casting / 4	PAN + PDMS	66	26.5	77.5	1 d
Casting / 5	F-42 (50 nm)	defective			1 d
Casting / 3	F-42 + silicone	165	16.7	38.9	6 d
		51	12.2	23.0	13 d
Casting / 3	F-42 + silicone	110	19.0	48.6	27 h
		81	12.1	33.3	50 h

SEM images of samples prepared on (PAN + PDMS) supports evidenced a PIM layer of 4-5 micron, depending on the polymer concentration in the coating solution (Figure 10). A good contact between the polymer and the support was revealed, without an intrusion of the PIM-EA(H_2)-TB into the support pores.

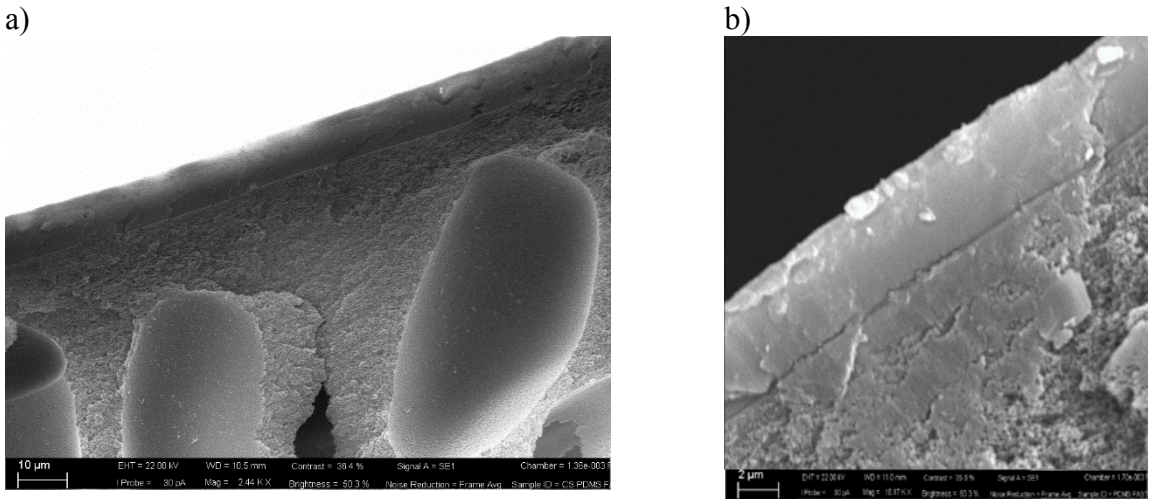

Figure 10. Cross-section of PIM-EA(H_2)-TB composite membranes prepared on (PAN + PDMS layer) flat-sheets. Polymer concentration in DCM: a) 3 wt.%; b) 4 wt.%.

3.2.3. HF composite membranes

The coating of HFs with PIM-EA(H_2)-TB solutions was more challenging. In the context of thin films, geometry has a crucial role. These highly curved supports presented adhesion issues.

The membranes prepared by the vacuum-assisted coating procedure on the untreated PAN-HFs were not selective in gas permeation tests. An optical microscope showed a polymer layer detached from the PAN support or some cracks in the case of the external coating. No macroscopic defects were evident in the case of the membranes prepared using an internal coating, but when cutting the fibres for their evaluation, the PIM layer was easily removed from the support.

The membranes prepared by coating with the PIM solution the HFs with a silicone layer in the bore side demonstrated a poor adhesion between the PIM and the support.

Therefore, also in this case, the partial hydrolysis of the PAN-HFs was considered to induce a better interaction with the coating polymer. The coating with PIM-EA(H_2)-TB carried out on the HFs internally functionalised was not successful. The polymer relaxation and, thus, a shrinking of the coating layer could be the reason of a poor adhesion when applying a coating layer on the inner surface of the HFs.

In general, the HFs that were externally dip-coated presented a better quality. Table 7 reports the data obtained from gas permeation tests on some representative samples.

Table 7. Permeation properties of some representative PIM-EA(H_2)-TB composite membranes prepared by external coating on PAN-based HFs (25 °C).

PAN HF support	Dip-Coating conditions				P_CO_2 (GPU)	$\alpha O_2/N_2$ (-)	$\alpha H_2/N_2$ (-)	$\alpha CO_2/N_2$ (-)
	T (°C)	Polymer conc. (wt.%)	Solvent	Time (s)				
Untreated	RT	0.5	DCM	90	53	0.97	3.60	1.30
Untreated	RT	3	DCM	30	0.2	0.88	1.85	0.65
Untreated	RT	3	DCM	180	0.13	-	1.33	1.24
Untreated	RT	3	DCM/hex 96/4	30	11	1.19	8.17	2.44
Untreated	RT	4	DCM	30	24	1.44	7.61	3.0
–COOH Funct. (NaOH 0.5 M, 1 h)	RT	4	DCM	30	33	1.47	7.30	3.0
–COOH Funct. (NaOH 0.5 M, 1 h)	RT	0.5	DCM/hex 96/4	30	44	0.95	3.67	0.94
Untreated	38	3	DCM/hex 96/4	30	22	1.03	4.86	1.41
Untreated	38	4	DCM	30	21	3.14	21.4	11.0
–COOH Funct. (NaOH 2 M, 26 h)	38	4	DCM	30	2.5	0.58	2.5	1.28
–COOH Funct. (NaOH 0.5 M, 1 h)	38	4	DCM	30	22	5.81	36.9	19.8
None, Dense membrane	*RT*	*3*	DCM	-	*1240**	*5.71*	*38.2*	*21.3*

*Permeability expressed in Barrer [1 Barrer = 10^{-10} cm^3 (STP) cm cm^{-2} s^{-1} $cmHg^{-1}$]

The dip-coating of untreated HFs with solutions at 3 wt.% for 30 s produced membranes with a low selectivity (CO_2/N_2<1), indicating that gas transport was determined by pore flow through skin layer defects. An increase in the coating time, keeping the polymer concentration at 3 wt.%, resulted in a slight improvement (CO_2/N_2>1). More dilute solutions (0.5 wt.%), considered to produce thinner layers, thus reducing the cohesive strength in the coating layer with respect to the adhesion on the support, resulted in a slight improvement in the selectivity and in larger permeance.

The addition of a small amount of a non-solvent (*n*-hexane) to the coating solution at 3 wt.%, intensifying the polymer entanglement, resulted in an improved selectivity combined to a better

permeance. Similar results were achieved using more viscous 'gel-like' solutions with a concentration of 4 wt.% in DCM only, due to a reduced polymer intrusion in the support. However, the permselectivity measured after coating the untreated HFs was not reaching the intrinsic value of PIM-EA(H_2)-TB.

The coating of functionalised HFs with 0.5 wt.% solutions containing also *n*-hexane did not provide selective samples. More concentrated PIM solutions (4 wt.%) applied onto functionalised HFs resulted in samples with similar selectivity than those produced on the untreated supports, but an increased permeance was found, probably due to the more dense porous structure of the COOH-PAN HFs, further reducing the polymer intrusion in the support pores.

Morphological analysis evidenced a better adhesion with the coating polymer for the COOH-PAN HFs with respect to the untreated supports (Figure 11), showing a less marked chromatic difference for the two layers.

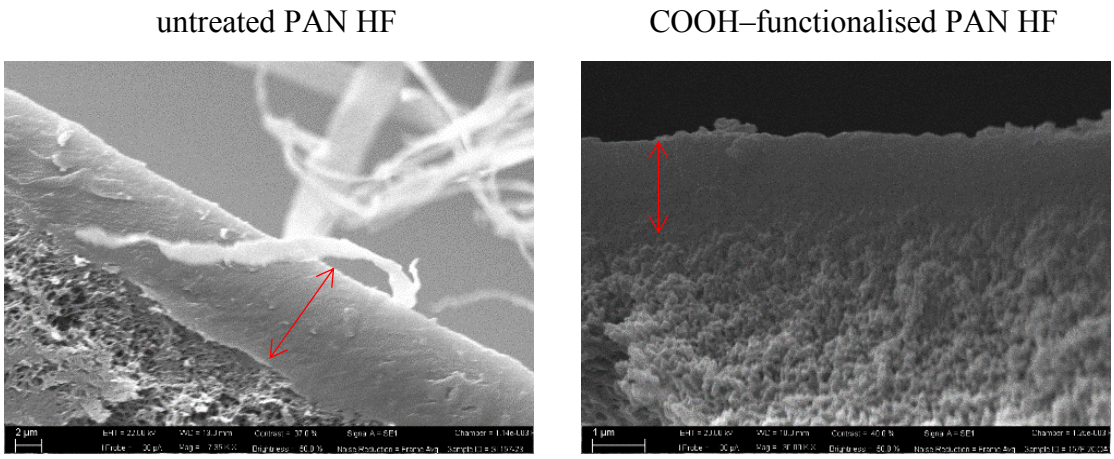

Figure 11. SEM images of the cross-section of PIM-EA(H_2)-TB composite membranes prepared by coating PAN-based HFs.

Solvent evaporation at ambient conditions produced films containing empty cells organised in a quite ordered hexagonal array and with pore size below 1 micron (Figure 12). SEM photomicrographs revealed micropores on the surface that did not grow in the coating layer. Similar arrays were described in the case of films prepared from the same solvent (DCM) solutions of polystyrene [61] or PES [62]. In that cases, water droplets condensed from water vapour were recognised as template for pore formation. Furthermore, in the case of Honeycomb-Patterned films the pore size increases with the decrease of the solvent volatility [63]. This confirm the interest in using DCM for preparing dense films.

The present study evidenced as condensation of humidity onto the air/polymer solution (in DCM) interface is responsible for the formation of surface pores, thus providing useful guidelines for the fabrication of films with controlled porosity and pore structure by using PIMs.

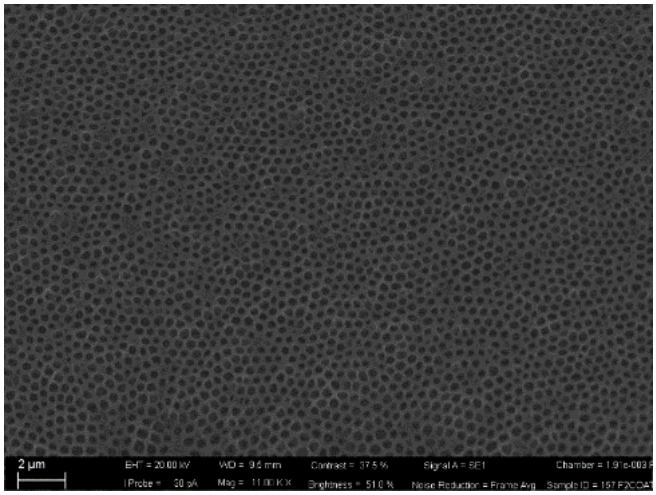

Figure 12. SEM images of the surface aspect of PIM-EA(H_2)-TB composite HFs membranes prepared by coating COOH-PAN HFs at room conditions.

To produce dense layers as required for gas separation, the dip-coating was performed in controlled temperature and humidity conditions. Condensation of the moisture on the polymeric surface is more likely in the case of a fast solvent evaporation at higher relative humidity [64]. An increasing relative humidity results in larger surface and overall porosity in films produced via the breath figure technique [65]. Therefore, a thermostatic chamber was used, working at ca. 38 °C (i.e., close to the boiling point of DCM) and RH < 30%. A synergistic positive effect was attained by increasing both the temperature and the polymer concentration in DCM (4 wt.%) and simultaneously reducing the relative humidity. The identified coating procedure produced better results on the untreated HFs, reaching selectivity values $\alpha\_CO_2/N_2 \sim 11.0$. The gas permeation tests confirmed the presence of a dense and selective layer of PIM-EA(H_2)-TB on PAN-HFs functionalised under mild conditions (NaOH, 0.5 M for 60 min) and then coated in a controlled environment (Table 7, penultimate row). In particular, this composite membrane keeps the intrinsic selectivity values for O_2/N_2, H_2/N_2 and CO_2/N_2 of the PIM-EA(H_2)-TB cast from DCM. This result is a useful starting point for the application of this novel PIM polymer in gas separations of industrial interest.

Conclusions

Dense self-supported films prepared from a novel polymer with intrinsic microporosity, PIM-EA(H_2)-TB, dissolved in chloroform or dichloromethane, show a noticeably high concentration of residual solvent. TGA analysis detects a dichloromethane amount of about 15 wt.% and chloroform amount of 25 wt.%. The dense films prepared using chloroform show a lower permeability than that prepared with dichloromethane. The strong interaction of the polymer matrix with chloroform,

confirmed by molecular modelling, leads to the partial saturation of the sorption sites and a competition between solvent and permeating gas molecules. The presence of both solvents leads to a decrease in the available free volume. The reduction is higher in films cast from chloroform with respect to those containing dichloromethane molecules. These results indicate that dichloromethane, having a satisfactory compatibility with PAN-based supports, is more suitable than chloroform as solvent for preparing composite membranes with PIM-EA(H_2)-TB. Flat-sheet and hollow fibre membranes were used as support. In the case of flat-sheet supports, a silicone gutter layer favours the formation of defect-free PIM-EA(H_2)-TB coatings. For PAN-based hollow fibres, spun *ad hoc*, the hydrolysis of nitrile groups to the corresponding –COOH groups enhances the compatibility with the PIM coating layers. Low relative humidity (less than 30%) at temperatures close to the dichloromethane boiling point (39.6 °C) prevents the formation of micropores on the membrane surface, as evidenced by a morphological analysis, producing homogeneous and dense layers. PIM-EA(H_2)-TB composite HFs, where the functionalisation of the PAN support was carried out in mild conditions, show the best permselective properties: polymer selectivity for O_2/N_2, H_2/N_2 and CO_2/N_2 gas pairs is close to that measured in dense films cast from dichloromethane.

Acknowledgements

The work leading to these results has received funding from the European Community's Seventh Framework Programme under grant agreement no. grant FP7-Energy-2013-1-608490, project M^4CO_2, "Energy efficient MOF-based Mixed Matrix Membranes for CO_2 Capture" and from the Italian Programma Operativo Nazionale Ricerca e Competitività 2007-2013, project "MicroPERLA", grant PON01_01840.

References

1. P. Bernardo, E. Drioli, Golemme, G. Membrane gas separation: a review/state of the art. *Ind. Eng. Chem. Res.* 48/10 (2009) 4638–4663.
2. B.D. Freeman, Basis of Permeability/Selectivity tradeoff relations in polymeric gas separation membranes, *Macromolecules* 32 (1999) 375–380.
3. P.M. Budd, E.S. Elabas, B.S. Ghanem, S. Makhseed, N.B. McKeown, K.J. Msayib, C.E. Tattershall, D. Wang, Solution-processed, organophilic membrane derived from a polymer of intrinsic microporosity, *Adv. Mater.* 16 (2004) 456–459.
4. a) L.M. Robeson, Correlation of separation factor versus permeability for polymeric membranes, *J. Membr. Sci*. 62 (1991) 165–185; b) L.M. Robeson, The upper bound revisited, *J. Membr. Sci*. 320 (2008) 390–400.
5. P.M. Budd, N.B. McKeown, Highly permeable polymers for gas separation membranes, *Polym. Chem.* 1 (2010) 63–68.

6. M. Carta, R. Malpass-Evans, M. Croad, Y. Rogan, J.C. Jansen, P. Bernardo, F. Bazzarelli, N.B. McKeown, Efficient Polymer-based molecular sieve membranes for membrane gas separations, *Science* 339 (2013) 303–307.
7. Tocci, E.; L. De Lorenzo, P. Bernardo, G. Clarizia, F. Bazzarelli, N.B. McKeown, M. Carta, Malpass-Evans, R.; K. Friess,; Pilnácek, K.; Lanč, M.; Y.P. Yampolskii, L. Strarannikova, V Shantarovich, M. Mauri, J.C. Jansen, Ethanoanthracene-based polymer of intrinsic microporosity from Tröger's base formation: detailed permeation properties and molecular modelling, *Macromolecules* 47(22) (2014) 7900–7916.
8. I. Pinnau, J.G. Wijmans, I. Blume, T. Kuroda, K.-V. Peinemann, Gas permeation through composite membranes, *J. Membr. Sci.* 37 (1988) 81–88.
9. T.S. Chung, E.R. Kafchinski, P. Foley, R.S. Kohn, R.S. Straff, Fabrication of composite hollow fibres for air separation, *J. Appl. Polym. Sci.* 53 (1994) 701–708.
10. R.W. Baker, Future directions of membrane gas separation technology, *Ind. Eng. Chem. Res*. 2 (2012) 1393–1411.
11. M.P. Achalpurkar, U.K. Kharul, H.R. Lohokare, P.B. Karadkar, Gas permeation in amine functionalized silicon rubber membranes, *Separ. Purif. Tech.* 57/2 (2007) 304–313.
12. J.-J. Shieh, T.-S. Chung, D.R. Paul, Study on multi-layer composite hollow fibre membranes for gas separation, *Chem. Eng. Sci.* 54 (1999) 675–684.
13. F. Bazzarelli, P. Bernardo, F. Tasselli, G. Clarizia, V.G. Dzyubenko, Vdovin, P. J.C. Jansen, Multilayer composite SBS membranes for pervaporation and gas separation, *Separ. Purif. Tech.* 80 (2011) 635–642.
14. J. Jansen, F. Tasselli, E. Tocci, E. Drioli, High-flux composite perfluorinated gas separation membranes of Hyflon® AD on a hollow fibre ultrafiltration membrane support, *Desalination* 192(1-3) (2006) 207-213.
15. N. Hernandez, J. Iniesta, V. Montiel Leguey, R. Armstrong, S.H. Taylor, E. Madrid, Y. Rong, R. Castaing, R. Malpass-Evans, M. Carta, N.B. McKeown, F. Marken, Carbonization of polymers of intrinsic microporosity to microporous heterocarbon: Capacitive pH measurements, *Applied Materials Today* 9 (2017) 136-144.
16. L. Shao, T.-S. Chung, G. Wensley, S.H. Goh, K.P. Pramoda, Casting solvent effects on morphologies, gas transport properties of a novel 6FDA/PMDA–TMMDA copolyimide membrane and its derived carbon membranes, *Journal of Membrane Science* 244/1–2 (2004) 77–87.
17. Y. Yampolskii, A. Alentiev, G. Bondarenko, Y. Kostina, M. Heuchel, Intermolecular Interactions: New way to govern transport properties of membrane materials, *Ind. Eng. Chem. Res*. 49 (2010) 12031–12037.
18. N. Chaukura, L. Maynard-Atem, Interaction of a Polymer of Intrinsic Microporosity (PIM-1) with penetrants, *American Journal of Applied Chemistry* 3(3) (2015) 139–146.
19. L. Zhang, W. Fang, J. Jiang, Effects of Residual Solvent on Membrane Structure and Gas Permeation in a Polymer of Intrinsic Microporosity: Insight from Atomistic Simulation, *J. Phys. Chem. C* 115 (2011) 11233–11239.
20. J. Weber, N. Du, M.D. Guiver, Influence of Intermolecular Interactions on the Observable Porosity in Intrinsically Microporous Polymers, *Macromolecules* 44 (2011) 1763–1767.
21. M.L. Zue, C.S. McKay, B.A. McCool, M.G. Finn, R.P. Lively, Effect of Nonsolvent Treatments on the Microstructure of PIM‐1, *Macromolecules* 48 (2015) 5780−5790.
22. P. M. Budd, N. B. McKeown, B. S. Ghanem, K. J. Msayib, D. Fritsch, L. Starannikova, N. Belov, O. Sanfirova, Y. Yampolskii, V. Shantarovich, Gas permeation parameters and other physicochemical properties of a polymer of intrinsic microporosity: polybenzodioxane PIM-1, *J. Membr. Sci*. 325 (2008) 851−860.

23. K.-S. Chang, C.-C. Tung, K.-S. Wang, K.-L. Tung, Free Volume Analysis and Gas Transport Mechanisms of Aromatic Polyimide Membranes: A Molecular Simulation Study, *J. Phys. Chem. B* 113 (29) (2009) 9821–9830.
24. D. Hofmann, M. Entrialgo-Castano, A. Lebret, M. Heuchel, Yu. Yampolskii, Molecular modeling investigation of free volume distributions in stiff chain polymers with conventional and ultrahigh free volume: comparison between molecular modeling and positron lifetime studies. *Macromolecules* 36 (2003) 8528–8538.
25. J.C. Jansen, M. Macchione, E. Tocci, L. De Lorenzo, Yu.P. Yampolskii, O. Sanfirova, V.P. Shantarovich, M. Heuchel, D. Hofmann, E. Drioli, Comparative study of different probing techniques for the analysis of the free volume distribution in amorphous glassy perfluoropolymers, *Macromolecules* 42 (2009) 7589–7604.
26. C.H. Park, E. Tocci, S. Kim, A. Kumar,; Y.M. Lee, E. Drioli, A Simulation Study on OH-Containing Polyimide (HPI) and Thermally Rearranged Polybenzoxazoles (TR-PBO): Relationship between Gas Transport Properties and Free Volume Morphology, *J. Phys. Chem. B* 118 (2014) 2746−2757.
27. Y. Rogan, R. Malpass-Evans, M. Carta, J.C. Jansen, P. Bernardo, G. Clarizia, E. Tocci, K. Friess, M. Lanc, N. B. McKeown, A highly permeable polyimide with enhanced selectivity for membrane gas separations, *Journal of Materials Chemistry A* 2 (2014) 4874–4877.
28. S. Darvishmanesh, J. Vanneste, E. Tocci, J.C. Jansen, F. Tasselli, J. Degreve, E. Drioli, B. Van der Bruggen, Physicochemical characterization of solute retention in solvent resistant nanofiltration: the effect of solute size, polarity, dipole moment, and solubility parameter, *J. Phys. Chem. B* 115 (2011) 14507–14517.
29. C.H. Park, E. Tocci, E. Fontananova, M.A. Bahattab, S.A. Aljlil, Drioli, E. Mixed matrix membranes containing Functionalized Multiwalled Carbon Nanotubes: Mesoscale Simulation and Experimental Approach for Optimizing Dispersion, *Journal of Membrane Science* 514 (2016) 195–20.
30. F. Tasselli, E. Drioli, Tuning of hollow fibre membrane properties using different bore fluids, *J. Membr. Sci*. 301 (2007) 11−18.
31. E. Esposito, G. Clarizia, P. Bernardo, J.C. Jansen, Z. Sedláková, P. Izák, S. Curcio, B.D. Cindio, F. Tasselli, Pebax®/PAN hollow fibre membranes for CO_2/CH_4 separation, *Chem. Eng. Process. Process Intensif.* 94 (2015) 53–61.
32. N.-W. Oh, J. Jegal, K.-H. Lee, Preparation and characterization of nanofiltration composite membranes using Polyacrylonitrile (PAN). I. Preparation and modification of PAN supports, *J. Applied Polymer Science* 80 (2001) 1854–1862.
33. J. Crank, The mathematics of diffusion, 2nd ed.; Clarendon Press, Oxford, 1975.
34. J.G. Wijmans and R.W. Baker, The solution-diffusion model: a review, *J. Membr. Sci*. 107 (1995) 1–21.
35. Accelrys Software Inc, P. U. G. P. s. BIOVIA (ex Material Studio 7.0) package. Classical simulation theory section. Amorphous Cell module. Sorption User Guide, (2013).
36. a) D.N. Theodorou, U.W. Suter, Detailed molecular structure of a vinyl polymer glass, *Macromolecules* 18 (1985) 1467–1478; b) D. N. Theodorou, U. W. Suter, Atomistic modeling of mechanical properties of polymeric glasses, *Macromolecules* 19 (1986) 139–154.
37. H. Sun, Ab initio calculations and force field development for computer simulation of polysilanes, *Macromolecules* 28(3) (1995) 701–712.
38. E. Tocci, P. Pullumbi A. Molecular simulation of realistic membrane models of alkylated PEEK membranes, *Molecular Simulation*, 32(2) (2006) 145-154.
39. C.H. Park, E. Tocci, Y.M. Lee, E. Drioli, Thermal Treatment Effect on the Polybenzoxazole (TR-PBO), *J. Phys. Chem. B* 116 (2012) 12864–12877.
40. T.A. Andrea, W.C. Swope, H.C. Andersen, The Role of Long Ranged Forces in Determining the Structure and Properties of Liquid Water, *J. Chem. Phys* 79 (1983) 4576–4584.

41. H.J.C. Berendsen, J. P. M. Postma, W. F. Van Gunsteren, A. Di Nola, J.R. Haak, Molecular-Dynamics with Coupling to an External Bath, *J. Chem. Phys.* 81 (1984) 3684–3690.
42. M. Heuchel, D. Hofmann, P. Pullumbi, Molecular Modeling of Small-Molecule Permeation in Polyimides and Its Correlation to Free-Volume Distributions, *Macromolecules* 37 (2003) 201–214.
43. J.M. Haile, *Molecular Dynamics Simulation*; Wiley: New York, NY, USA, 1992.
44. N. Metropolis, A.W. Rosenbluth, M.N. Rosenbluth, A.H. Teller, E. Teller, Equation of state calculations by fast computing machines, *J. Chem. Phys.* 21 (1953) 1087–1092.
45. M.P. Allen, DJ. Tildesley, Computer simulation of liquids. New York: Oxford; 1987.
46. A. J. Bondi, van der Waals volumes and radii, *J. Phys. Chem.*,68 (1964), 441– 451
47. C. Joly, D. Le Cerf, C. Chappey, D. Langevin, G. Muller, Residual solvent effect on the permeation properties of fluorinated polyimide films, *Separation and Purification Technology* 16/1 (1999) 47–54.
48. Y. Huang, D.R. Paul, Effect of film thickness on the gas-permeation characteristics of glassy polymer membranes, *Ind. Eng. Chem. Res*. 46(8) (2007) 2342–2347.
49. J.H. Hildebrand, J.M. Prausnitz, R.L. Scott, Regulated and Related Solutions, Van Nostrand Reinhold Co., New York, 1970.
50. N. Chaukura, L. Maynard-Atem, Interaction of a Polymer of Intrinsic Microporosity (PIM-1) with Penetrants, *American Journal of Applied Chemistry* 3/3 (2015) 139–146.
51. Y. Maeda and D.R. Paul, Effect of antiplasticization on selectivity and productivity of gas separation membranes, *J. Membr. Sci.* 30 (1987) 1–9.
52. M. Macchione, J.C. Jansen, G. De Luca, E. Tocci, M. Longeri, E. Drioli, Experimental analysis and simulation of the gas transport in dense Hyflon® AD60X membranes: Influence of residual solvent, *Polymer* 48 (2007) 2619–2635.
53. M.D. Guiver, Y.M. Lee, Polymer Rigidity Improves Microporous Membranes, *Science* 339/6117 (2013) 284–285.
54. K. Shirono, T. Morimatsu, F. Takemura,Gas Solubilities (CO_2, O_2, Ar, N_2, H_2 He) in Liquid Chlorinated Methanes, *J. Chem. Eng. Data* 53 (2008) 1867–1871.
55. D.W. Breck, Zeolite Molecular Sieves: Structure, Chemistry and Use. John Wiley & Sons, Inc.: New York, 1974.
56. Y. Yampolskii, Polymeric gas separation membranes, *Macromolecules* 45 (2012) 3298−3311.
57. S. Neyertz, D. Brown, S. Pandiyan, N.F.A. van der Vegt, Molecular Modelling of Oxygen and Carbon Dioxide Permeation in Glassy Polymer Membranes, *Macromolecules* 43 (2010) 7813−7827.
58. X. Ma, I. Pinnau, Effect of Film Thickness and Physical Aging on “Intrinsic” Gas Permeation Properties of Microporous Ethanoanthracene-Based Polyimides, *Macromolecules* 51 (2018) 1069–1076.
59. C.L. Staiger, S.J. Pas, A. J. Hill, C.J. Cornelius, Gas Separation, free volume distribution, and physical aging of a highly microporous spirobisindane polymer, *Chem. Mater.* 20(8) (2008) 2606–2608.
60. P. Bernardo, F. Bazzarelli, F. Tasselli, G. Clarizia, C.R. Mason, L. Maynard-Atem, P.M. Budd, M. Lanč, O. Vopička, K. Pilnáček, K. Friess, D. Fritsch, Yu.P. Yampolskii, V. Shantarovich, J.C. Jansen, Effect of physical aging on the gas transport and sorption in PIM-1 membranes, *Polymer* 113 (2017) 283-294
61. T. Nishio, M. Kashiwagi, K. Miyazaki, M. Yahiro, C. Adachi, Preparation under High Humidity Conditions of Nanoporous Polymer Film with 80nm Minimum Pore Size, *Applied Physics Express* 3 (2010) 025201–025203.
62. Y. Liu, H. Ma, Y. Tian, F. Xie, X. Wang, Fabrication of Durable Honeycomb-Patterned Films of Poly(ether sulfone)s via Breath Figures, *Macromolecular Chemistry and Physics* 215 (2014) 1446−1455.

63. Y. Tian, S. Liu, H. Ding, L. Wang, B. Liu, Y. Shi, Formation of Honeycomb-Patterned Polyetherketone Cardo (PEK-C) Films in a Highly Humid Atmosphere, *Macromol. Chem. Phys.* 207 (2006) 1998–2005.
64. G.-T. Kim, J.-S. Lee, J.-H. Shin, Y.-C. Ahn, Hwang, Y.-J.; Shin, H.-S.; Lee, J.-K.; Sung, C.-M. Investigation of Pore Formation for Polystyrene Electrospun Fibre: Effect of Relative Humidity, *Korean J. Chem. Eng*. 22(5) (2005) 783–788.
65. A. Gugliuzza, M.C. Aceto, F. Macedonio, E. Drioli, Water droplets as template for next-generation self-assembled poly-(etheretherketone) with cardo membranes, *J. Phys. Chem. B*. 112 (2008) 10483–10496.

Supplementary Information

a)

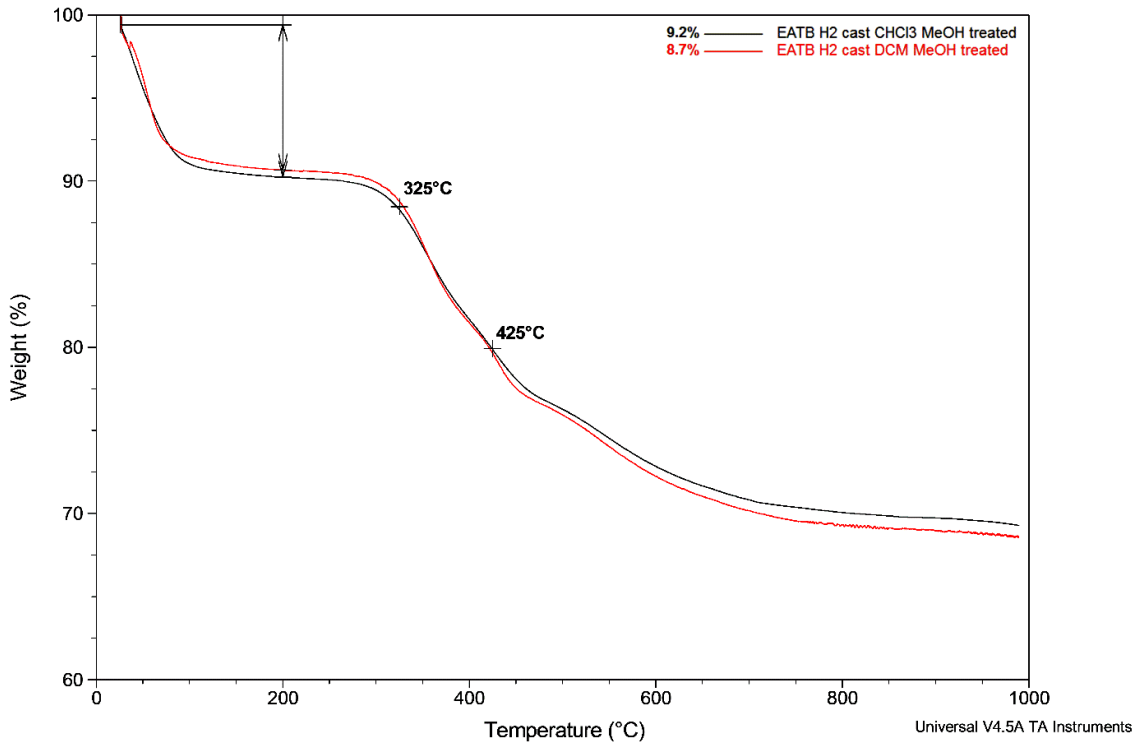

b)

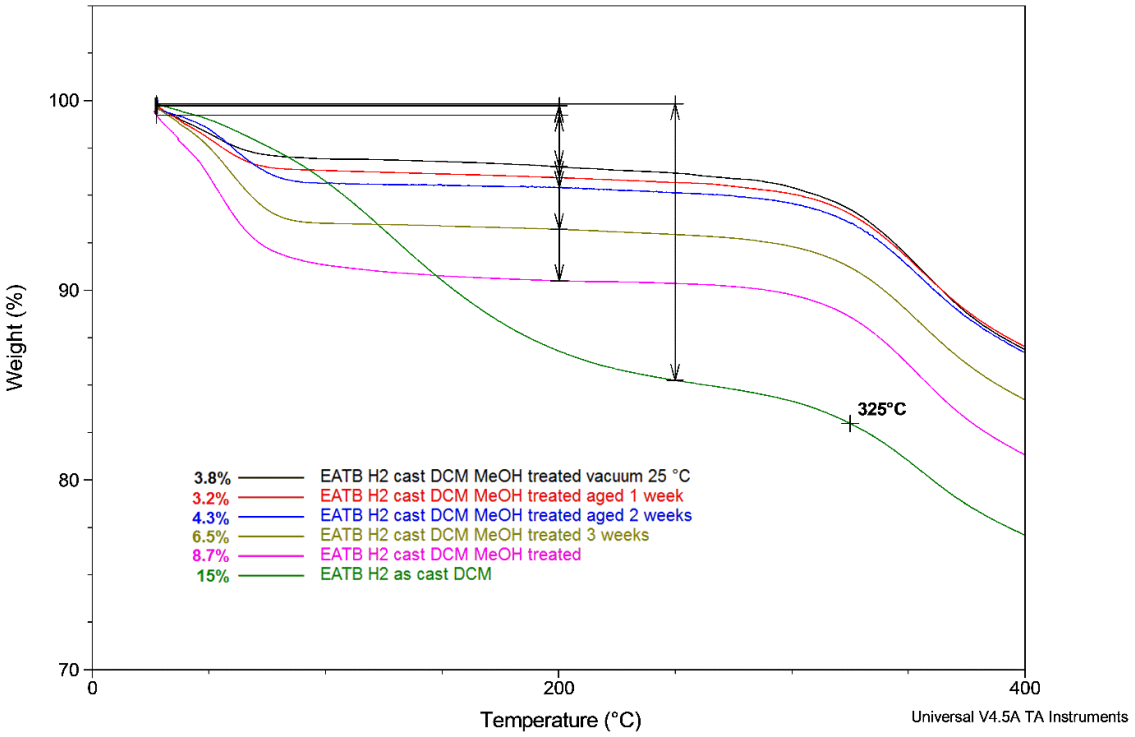

Figure S1. TGA of PIM-EA(H_2)-TB films.
a) overlay of two films cast from $CHCl_3$ or DCM and MeOH-treated; b) overlay of a film cast from DCM, MeOH-treated and aged, zoom.

Table S1. Permeation properties measured on dense 'as-cast' films of PIM-EA(H_2)-TB prepared in DCM or $CHCl_3$. T = 25 °C and feed pressure = 1 bar.

Solvent / thickness		**CO_2**	**H_2**	**CH_4**	**He**	**O_2**	**N_2**
DCM / 83 micron	**Permeability** (Barrer)	1240	2220	75	955	332	58
	D (10^{-12} m^2 s^{-1})	15.0	2920	3.26	5100	65.4	13.0
	S (cm^3 cm^{-3} bar^{-1})	62.0	0.57	17.3	0.14	3.80	3.36
	Ideal selectivity, gas/N_2 (-)	21.3	38.2	1.30	16.4	5.71	-
$CHCl_3$ / 129 micron	**Permeability** (Barrer)	495	262	64	118	94	29
	D (10^{-12} m^2 s^{-1})	13.7	803	6.35	2010	40.4	16.3
	S (cm^3 cm^{-3} bar^{-1})	27.1	0.24	7.54	0.043	1.74	1.34
	Ideal selectivity, gas/N_2 (-)	17.1	9.01	2.20	4.05	3.23	-

1 Barrer = 10^{-10} cm^3 cm cm^{-2} $cmHg^{-1}$ s^{-1}